The role of Axl in melanoma metastasis

By

Jing Kang

This thesis is submitted in partial fulfillment of the requirements for the degree of Master of Science

University of Bergen

The Department of Biomedicine

Bergen, Norway

June 2015

Acknowledgements

The work present in this thesis was carried out as part of the Master of Science degree in Medical Cell Biology at the Department of Biomedicine, University of Bergen, in the period August 2013 to June 2015. The laborious work was carried out at CELLNET group.

First of all I would like to thank my main supervisor James B. Lorens for excellent scientific guidance and support throughout this period. I am so grateful for everything I have learned and for the opportunity to be a part of your fantastic lab. I also wish to thank my co-supervisor Niels Aarsæther for always being helpful and supportive, both in the lab and in the writing process. I have greatly appreciated all the advices and encouragement. I am also grateful for getting the opportunity to do my thesis on such an interesting and up to date field, with highly competent people.

I will thank Kjersti Davidsen, Gry Sandvik Haaland, David Micklem, Magnus Blø and Sissel Vik Berge for their supports and guidance in the lab and for always being beyond positive, enthusiastic and helpful. I also like to thank Maren Stallemo and Stian Krog for their help, patience and support. I also express my gratitude to all people who have helped and encouraged me during my master study.

Finally I will thank my wonderful family for always providing love, care and support.

Bergen 2015

Jing Kang

Contents

Abbreviations

Akt	Protein kinase B (PKB)
BSA	Bovine serum albumin
Cas	CRISPR-associated
Cas9n	Cas9 nickase mutant
CI	Cell index
CIM	Cell invasion/migration
CP	Crossing Point
CRISPR	Clustered regularly interspaced palindromic repeats
crRNA	CRISPR RNA
DMSO	Dimethyl sulfoxide
DP	Dual-plate
DSBs	Sequence-specific double-strand breaks
ECM	Extracellular matrix
EDTA	Ethylenediaminetetraacetic acid
EGFR	Epidermal growth factor receptor
EMT	Epithelial–mesenchymal transition
ERK	Extracellular signal-regulated kinase
FBS	Fetal Bovine Serum
FITC	Fluorescein isothiocyanate
GAPDH	Glyceraldehyde 3-phosphate dehydrogenase
Gas6	The growth arrest–specific gene 6
GFP	Green fluorescent protein
MAPK	Mitogen-activated protein kinases
MEK	Mitogen-activated protein kinase kinase
α-MEM	α-modified minimal essential medium
MITF	Microphthalmia-associated transcription factor
NHEJ	Non-homologous end joining
HCC	Hepatocellular carcinoma
HDR	Homology-directed repair
HER-2	Receptor tyrosine-protein kinase erbB-2
OS	Overall survial
PBS	Phosphate buffered saline
PD-1	Anti-programmed death-1
PFS	Progression-free survival
PKB	Protein kinase B
PIP3	Phosphatidylinositol (3,4,5)-trisphosphate
PI3K	Phosphatidylinositol 3-kinase
PMSF	Phenylmethylsulfonyl fluorid
PTEN	Phosphatase and tensin homolog
RTCA	Real-time cell-sensing assay
STAT3	Signal transducer and activator of transcription 3
SD	Standard Deviation
SDS	Sodium dodecyl sulfate
TALENs	Transcription activator–like effector nucleases
TEMED	Tetramethylethylenediamine
tracrRNA	transactivating RNA
ZFNs	Zinc-finger nucleases

Abstract

Melanoma is a highly invasive and metastatic cancer which can originate in skin, mucosa, uvea and leptomeninges. Although only 4% of skin cancers are melanomas, it leads to nearly 80% of skin cancer-related deaths. Melanoma metastasizes quickly, and the median overall survival of metastatic melanoma is less than one year. Unfortunately, the under-lying biological mechanisms manipulating melanoma development and metastasis have not been clarified, thus understanding the mechanism of melanoma metastasis is a major issue.

The receptor tyrosine kinase Axl, which belongs to the TAM family, has a single ligand growth arrest–specific gene 6 (Gas6). Axl signaling enhances many essential biological functions for cancer progression by influencing cell transformation, proliferation, invasion, metastasis, survival, angiogenesis, and resistance to chemotherapeutic and targeting drugs. Furthermore, Axl correlates with cell migration and invasion in melanoma. It is reported that about 40% of melanoma cell lines express high Axl levels, and the frequency of Axl expression increased with disease progression.

The Akt family, which is the serine/threonine-specific protein kinase family, has three isoforms Akt1, Akt2 and Akt3, although they are closely related and highly conserved, it was revealed that they possessed distinct functions. Akt3 is the predominant isoform in melanomas where it plays a key role in melanoma development including invasion, metastasis and therapeutic resistance.

The Axl-Akt3 co-expression is apparent in gene expression data sets, and Axl signaling regulates the EMT gene program by activating nuclear-localized Akt3 in breast cancer. A hypothesis model of Axl-dependent EMT gene program maintenance via activation of nuclear Akt3 was previously proposed by our research group indicating that Axl-Akt3 signaling may play an important role in breast cancer progression and Axl-Akt3 signaling pathway may become a novel therapeutic target to treat advanced breast cancer.

In this study, the central hypothesis is that Axl affects melanoma metastasis via activation of Akt3, and the objectives including: characterize the role of Axl in metastatic melanoma; elucidate the mechanism for how Axl-Akt3 signaling affects metastasis in melanoma and validate the central hypothesis.

New Zealand Melanoma cell lines were obtained from Dr. Bruce Baguley (Auckland, NZ). QPCR and Western blot analysis was performed to measure the Axl and Akt3 expression. xCelligence system, an electronic real-time cell-sensing assay (RTCA), was used to analyze the cell functions including proliferation, migration and invasion (Matrigel); all the function analysis experiments were performed twice with the RTCA station separately in a normal incubator with atmospheric oxygen tension (21% O_2) and a low oxygen incubator with physiological oxygen tension (5% O_2); in migration assay we use higher FBS concentration to stimulate cells migrating; in invasion assay, we coated the CIM-Plate with matrigel and stimulated cells moving with different FBS concentration. Axl and Akt3-targeting CRISPR-

Cas9 plasmids were constructed (with D. Micklem) and sequence verified. Transfection was performed by Neon transfection system and analyzed by fluorescence microscopy.

We demonstrated that among our six New Zealand Melanoma cell lines, cells with higher expression of Axl have higher levels of proliferation, migration and invasion; Cells with higher expression of Akt3 also have higher abilities of proliferation and migration, but have the lowest invasion ability without co-expression of Axl. We found that cells kept in normal incubator (atmospheric, 21% O_2) and in low oxygen incubator (physiological, 5% O_2) showed different proliferation and invasion abilities, but similar migration level. In order to elucidate how Axl signaling contributes melanoma metastasis we tried to permanently knock out the gene coding for Axl using CRISPR-Cas9 system. However, so far we have not been able knock out the gene coding for Axl using this system in NZM17 cells.

In conclusion, Axl and Akt3 expression varied in among the New Zealand Melanoma cell lines. The Axl-Akt3 co-expressing NZM17 cells show consistent proliferation, migration and invasion abilities both physiological oxygen tension. NZM cells cultured at different oxygen tensions show differences in proliferation migration and invasiveness. Isolation of Axl CRISPR knock out NZM cell lines is in progress. These results support new therapeutic approaches based on Axl signaling inhibition to treat metastatic melanoma.

Introduction

1.1 Melanoma

1.1.1 Melanoma

Melanoma is a highly invasive and metastatic cancer which can originate in skin, mucosa, uvea, and leptomeninges [1]. Although only 4% of skin cancers are melanomas, it leads to nearly 80% of skin cancer-related deaths [2]. The incidence of melanoma has continued to increase, which made melanoma become the 5th most common cancer in men and the 6th most common in women [3]. Besides, according to the World Health Organization, about 132,000 new cases of malignant melanoma are diagnosed globally each year and the number is increasing at a faster rate than any other forms of cancer [4, 5]. At the same time, the mortality rate of melanoma also sharply increased in the last ten years worldwide [6]. Norway is actually worse off in this respect, as Norway has a higher mortality rate than countries with similar incidence rates, and has the same mortality rate as Australia, where the incidence rate is 2x of the Norwegian [7, 8]. Operative treatment of early-stage melanoma brings about a cure rate of 90%, but the average five-year survival rate of metastatic melanoma is around 11%, and the median survival rate is about 6 to 12 months [9]. The etiology and pathogenesis of melanoma is not yet fully known, some risk factors for the development of melanoma include sun exposure [10], presence of atypical nevi [11, 12], skin pigmentation phenotype [11], personal [12] and family histories [11] of melanoma. The most noteworthy part is the role of sun exposure and skin pigmentation phenotype, as they are well established risk factors. Intermittent intense sun exposure increases risk of melanoma and as opposed to chronic sun exposure that increases risk of other skin malignancies.

1.1.2 Metastatic melanoma

Cancer metastasis is the cause of approximately 90% of tumor deaths [15]. According to the ‘‘seed and soil’’ hypothesis, cancer metastatic cells function as ‘‘seeds’’ and a particular organ microenvironment or niche serves as the ‘‘soil’’ [16]. It is a multistep cascade requiring diverse biological processes, including local invasion/matrix remodeling, intravasation/extravasation, survival in circulation, and colonization, survival, and growth in secondary sites [17].

Melanoma metastasis is also a complex process requiring melanoma cell detachment from the primary tumor and migration to secondary sites in the body through the lymphatic or blood circulatory systems [18, 15]. Melanoma has the propensity to spread throughout the body even at early stages of tumorigenesis [19]. Staging of primary melanomas together with histopathological features such as thickness, mitotic index, ulceration, and lymph node status are generally prognostic of clinical outcome [20–24]. However, when melanoma cell dissemination occurs from primary tumors, it is difficult to diagnosis. Besides even patients with localized melanoma are diagnosed at stage I or II, approximately 7% or 30% will suffer a recurrence [25], and most will then progress to metastatic disease and eventual death [26].

Metastasis is the essential event dictating poor outcome for patients diagnosed with a localized primary melanoma.

1.1.3 The treatment of melanoma

The treatments of melanoma include surgery, chemotherapy, immunotherapy, and radiation therapy [27], however it is well known that melanoma is characteristically refractory to current therapies, so new approaches and therapies are needed to raise the life expectancy of patients with metastatic melanoma. In recent years, based on the improved understanding of genetic and molecular mechanism of melanoma, many new drugs were approved for treatment of advanced melanoma, including T-cell regulatory immune therapies for example the human anti-cytotoxic T lymphocyte antigen-4 monoclonal antibodies (ipilimumab) [28], anti-programmed death-1 (PD-1) antibodies (pembrolizumab, nivolumab) [29] and targeted therapies against MAPK pathway for example BRAF inhibitors (vemurafenib, dabrafenib) [30, 31], MEK inhibitor (trametinib) [32] and recently the combination of BRAF and MEK inhibitors (dabrafenib with trametinib) [33].

In particular, because 50% of melanomas have mutations in BRAF and up to 20% of melanomas have mutations in the NRAS gene in a mutually exclusive way with BRAF [34], there has been remarkable progress for the BRAF mutant subset of melanoma with the development of the selective BRAF and MEK inhibitors. For example, BRAF inhibitors alone produce response rates in the range of 40-50% with a median progression-free survival (PFS) of 6-7months [30, 31]; MEK inhibitor trametinib demonstrated significantly improved response rates (22 vs 8%) median PFS (4.8 vs 1.5 months) and 6-month overall survival (OS) (81 vs 67%) compared with chemotherapy in a Phase III clinical trial [32]; the combination of BRAF with MEK inhibitors resulted in more frequent responses and improved PFS and OS compared to BRAF inhibitors alone [33,35,36]. However, they all acquired resistance which seriously influenced the results of treatment, besides selection and appropriate sequencing of these drugs still remained challenging, following more research work of treatment is still eagerly needed.

1.2 Axl

1.2.1 Axl

The receptor tyrosine kinase Axl, which is a transmembrane receptor, was first identified as a transforming gene in chronic myeloid leukemia from two patients [37]. Axl, also called Ark and Ufo, contains an intracellular (C-terminal) kinase domain including three autophosphorylation sites (Tyr779, Tyr821, and Tyr866) and a unique extracellular (N-terminal) domain composed of two N-terminal immunoglobulin-like domains and two fibronectin type III repeats similar to the structure of neural cell adhesion molecules [38, 39]. Together with Tyro-3 and Mer, Axl belongs to the TAM family which has two ligands including protein S and the growth arrest–specific gene 6 (Gas6) [40], and Gas6 which is dependent on vitamin K has the highest affinity to Axl. Activation of Axl occurs after the binding to Gas6 [41; 42]

Previous studies have demonstrated that Axl has the oncogenic activity. It was reported that activation of Axl signaling by its ligand Gas6 leads to enhanced proliferation, survival, invasion, and metastasis of cancer cells. Furthermore Axl was found deregulated in several types of cancer, such as prostate [43; 44], breast [45], lung [46-48], leukemia [49; 50], and esophageal adenocarcinomas [49], and it has been shown to play a role in the epithelial–mesenchymal transition (EMT), which is also an important feature for the initiation of metastasis [51-55]. For example, in hepatocellular carcinoma (HCC), Axl was found up-regulation in situ hybridization and a further study suggested that Axl acts downstream of the Hippo pathway to trigger cell invasion and metastasis [56, 57]; in breast carcinoma, autocrine activation of Axl is reported essential for EMT and metastatic dissemination [52] and antagonizing Axl signaling inhibits pulmonary metastasis [45]. Besides overexpression of Axl is correlated with poor survival of tumor patients [58] and is also linked to an increase in resistance to various drug treatments [59-60]. For instance, imatinib-resistant gastrointestinal stromal tumors, nilotinib-resistant chronic myeloid leukemia cells, BMS-754087–resistant rhabdomyosarcoma, erlotinib-resistant EGFR-mutant lung cancer and lapatinib-resistant HER-2–positive breast tumor cells are all reported to link with increased Axl expression level [59-60; 63-65]. In this way, it also means that inhibition of Axl may prevent or overcome acquired resistance to certain drugs.

1.2.2 Signaling pathway of Axl

Axl signaling enhances many essential biological functions for cancer progression, chronic immune disorders and cardiovascular diseases by influencing cell transformation, proliferation, invasion, metastasis, survival, angiogenesis, and resistance to chemotherapeutic and targeting drugs [66-67]. Because Gas6 has the highest affinity for Axl among the TAM receptors [41-42], it is often called the Gas6/Axl pathway, which has been predominantly studied in cancer [67; 68]. Adequate evidence supported that the downstream pathways activated by the Gas6/Axl signaling include the phosphatidylinositol 3-kinase (PI3K)/Akt pathway [69], MAPK/extracellular signal-regulated kinase (ERK) pathway [70], and NF-κB pathway [71].

Several reports highlighted that PI3K/Akt pathway is the important downstream pathway activated by the Gas6/Axl signaling [72,73], which is involved in many cellular processes including proliferation, differentiation, apoptosis, cell cycle progression, cell motility and tumorigenesis, tumor growth, and angiogenesis [74, 75]. In addition, it is also reported that targeting PI3K/Akt inhibits proliferation and tumorigenesis of human cancer [73]. Besides, Xu J et al. found that Axl had a critical role in the PI3K/Akt-PAK1 signal pathway and knockdown of it inhibits the metastasis properties of hepatocellular carcinoma [76]. The implications of Axl and Akt in cancer progression have been reviewed by Korshunov, V.A. [67], where he suggests that activation of PI3K and its downstream target is a central step in Axl-dependent signal transduction. (**Figure 1**)

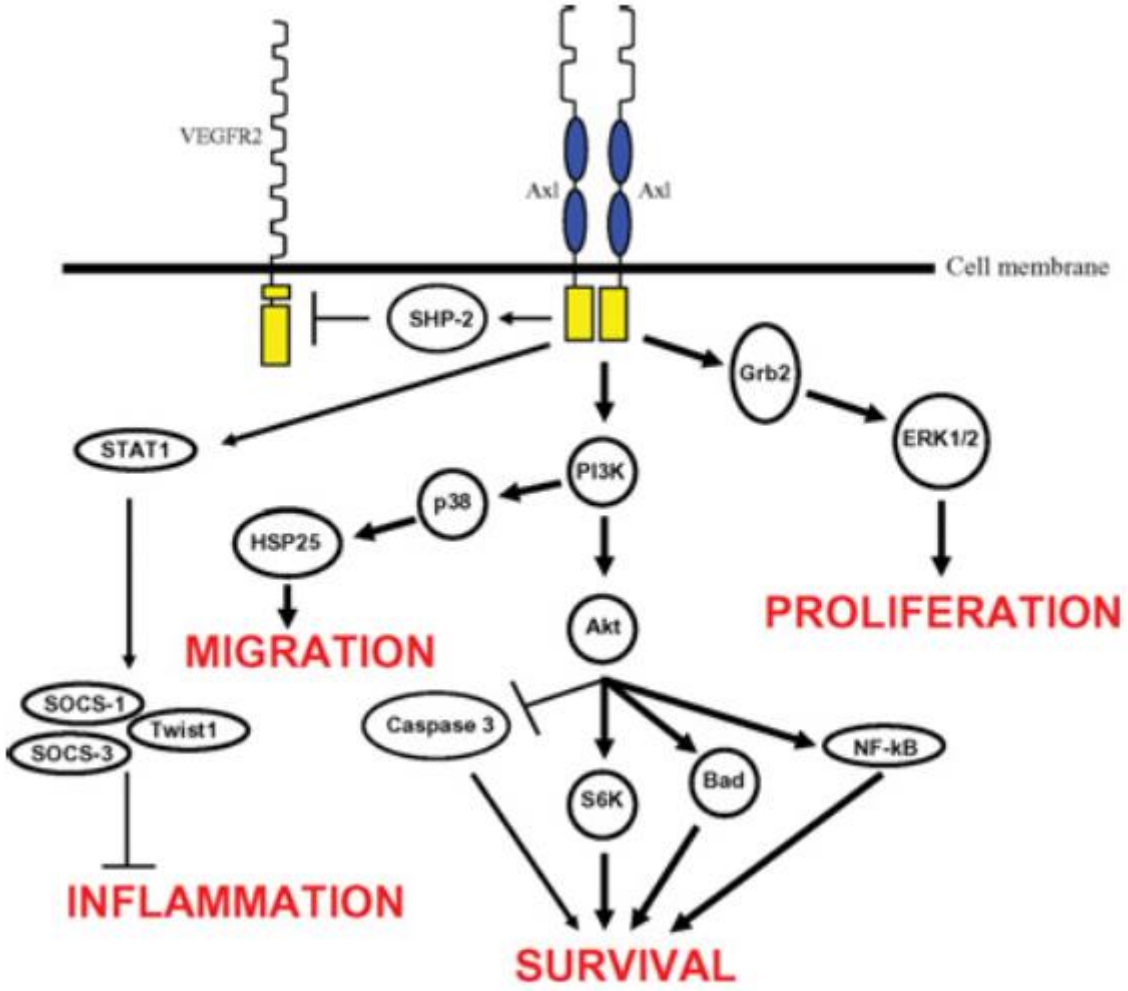

Figure 1: Axl receptor signal transduction. Axl signaling pathway controls biological functions such as inflammation, migration, survival and proliferation via activating STAT1, PI3K, Grb3 and other downstream proteins. Adapted from Reference [67].

1.2.3 Axl and melanoma

The role for Axl in melanoma has been studied for many years, however the importance of which has not been clearly elucidated. Sensi et al. have reported that 22 of 58 of cell lines (38%) in a melanoma progression panel were detected with high Axl expression, and they also found that the frequency of Axl expression increased with disease progression. Besides they found that Axl promoted tumor cell migration and invasion. Furthermore, knockdown or pharmacological inhibition of Axl using the selective inhibitor R428 showed comparable effects in reducing migration and invasion [77]. However, according to their research, Axl depletion did not dramatically affect proliferation [77].

In accordance to Sensi et al., Tworkoski et al. reported that inhibiting Axl function in a high Axl-expressing melanoma cell line with short interfering RNAs or a pharmacological inhibitor led to reduced invasion and migration [78]. However, in contrary to Sensi et Al.,

their data indicates that knockdown of Axl inhibits proliferation in some lines [77, 78]. All the results indicate that Axl may play an important role in melanoma metastasis, thus understanding the mechanism of how Axl affects melanoma metastasis is a major issue.

1.3 Akt3

1.3.1 Akt3

The Akt family, which is the serine/threonine-specific protein kinase family, has three isoforms Akt1, Akt2 and Akt3, they are encoded by different genes, but share a conserved domain structure consisting of an N-terminal pleckstrin homology domain, a kinase domain and a C-terminal regulatory domain containing a hydrophobic motif [80]. Although they are closely related and highly conserved, it was revealed that they possessed distinct functions in cancer models [81, 82]. Akt1 is ubiquitously expressed and is essential for growth [83, 84]; Akt2 is primarily expressed in insulin-responsive tissues and is essential for cell survival, growth and glucose homeostasis [83, 85]; Akt3 is highly expressed in brain and testes, and is essential for maintenance of brain homeostasis [83, 86, 87].

Akt3 is located at chromosome 1q44 and encodes the 479 amino acid [88]. Interestingly, about Akt3 there are different results reported in tumor progression, some believe that Akt3 can enhance tumor development. For example, recently, Turner, K. M et al. identified Akt3 as the dominant Akt isoform that robustly stimulates glioma progression, besides they also discovered key roles for Akt3 in activating DNA repair pathways, which led to enhanced survival of human glioblastoma cells following radiation or temozolomide treatment [89]. In contrast, there are also some evidences suggesting that Akt3 exerts inhibitory effects in cancer [83], for instance, it is reported that Akt3 has been shown to inhibit lung tumor growth in mice; inhibiting Akt3 can lead N-Cadherin to promote breast cancer metastasis [90–92].

1.3.2 Signaling pathway of Akt3

The PI3K/Akt pathway serves as a key factor in the regulation of cancer cell invasion and metastasis [93]. Akt3 was involved in PI3K and MAPK signaling pathway which can regulate cell senescence, proliferation and apoptosis. Besides, loss of Phosphatase and tensin homolog (PTEN) leads to increased levels of Phosphatidylinositol (3,4,5)-trisphosphate (PIP3) then increased activity of Akt3 [94-96]. The activated Akt3 inhibits apoptosis and induces proliferation by phosphorylation of substrate proteins (**Figure 2**) [97]. Furthermore, decreased apoptpsis makes melanoma cells less sensitive to chemotherapeutic drugs which function through this mechanism [97].

Recently, Akt3 and V600E BRAF have been cooperatively shown to promote melanoma development. Akt3 reduces its and MAPK pathway activity by phosphorylating mutant V600E BRAF in order to promote rather than inhibit growth. In other words, activating V600E BRAF mutation initially promotes nevi development, but the resulting high, intense activation of the MAPK pathway inhibits further tumor progression requiring Akt3 activation

to phosphorylate V600E BRAF to bypass this barrier and promote melanoma development [98].

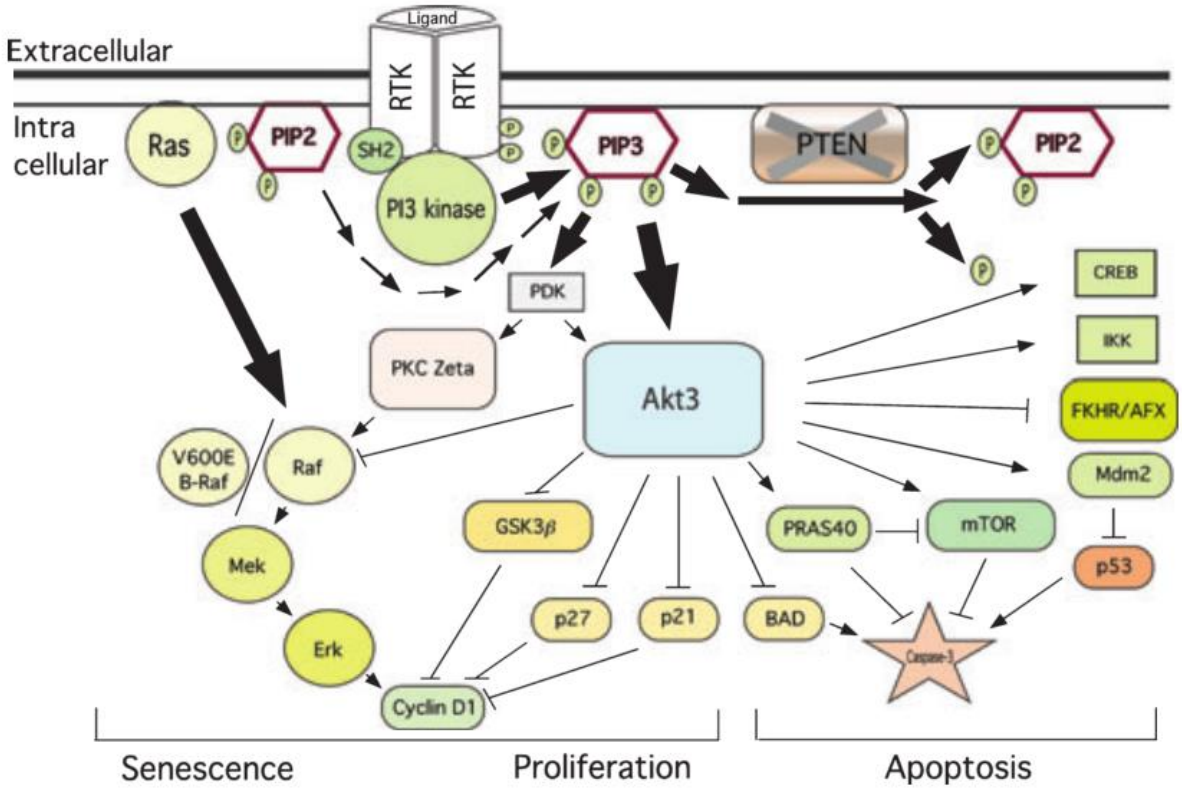

Figure 2: Akt3 was involved in PI3K and MAPK signaling pathway which can regulate cell senescence, proliferation and apoptosis. Adapted from Reference [97].

1.3.3 Akt3 and melanoma

Akt3 is the predominant isoform in melanomas where it plays a key role in melanoma development including invasion, metastasis and therapeutic resistance [96, 99]. Increased Akt3 expression/activity occurs in 60–70% of sporadic melanomas [96, 100] and also plays a significant role in progression to more advanced aggressive tumors [101, 94, 96]. The function of Akt3 in melanoma was widely studied, for example, an experimental tumor progression model in which Akt3 activity in melanocytes was compared with low passage cell lines from primary melanoma tumors at the radial and vertical stages of cell growth, revealed that Akt3 activity increased in the radial growth phase and remained elevated in comparison to Akt1 and Akt2. The high level of involvement in advanced melanomas leads to the inference that Akt3 activation performs critical functions in melanoma development [94, 96]. Acquisition of Akt3 activity facilitates the progression of quiescent melanocytic nevi into aggressive vertical and metastatic stages by inhibiting V600E BRAF activity thereby releasing cells from senescence block [97].

1.4 A model of Axl signaling via activation of Akt3

Recently, Tiron et al.in our research group proposed a hypothesis model of Axl-dependent EMT gene program maintenance via activation of nuclear Akt3 (**Figure 3**) [102]. This hypothesis model was based on breast cancer. They found that Akt3 was upregulated by EMT and required for Axl-dependent regulation of mammary stem cell traits, besides they also concluded that EMT and stem cell functions required Axl-dependent activation of nuclear targeted Akt3 [102]. In this hypothesis model, Axl and Akt3 expression are induced by micro-environmental factors and establish a novel signal transduction pathway activated by paracrine sources of Gas6. Their results implicated the Axl-Akt3 signaling pathway may become a novel therapeutic target to treat advanced breast cancer.

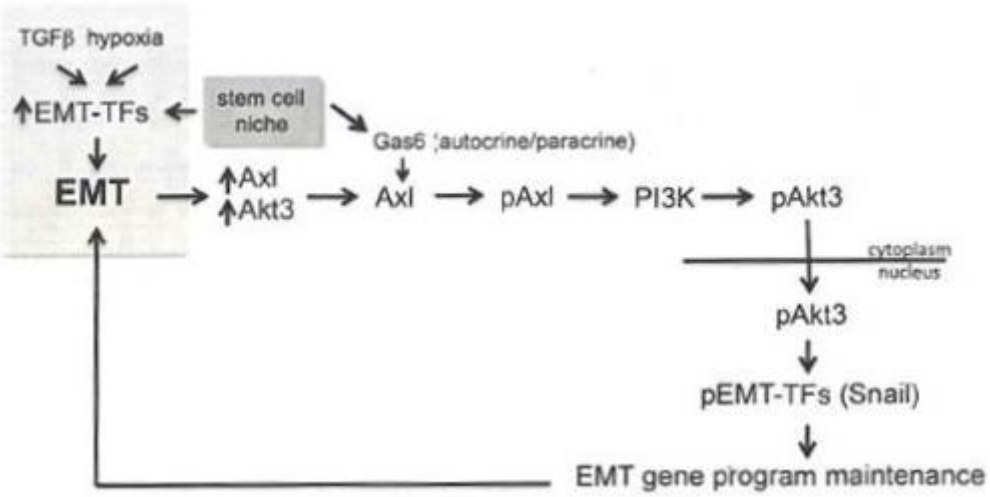

Figure 3: Hypothesis model of Axl affect cell functions via activation of Akt3. This hypothesis model was based on breast cancer. Adapted from Reference [102].

Hypothesis and aims

The central hypothesis is that Axl affects melanoma metastasis via activation of Akt3.

The aims of the study are:

Aim 1 Characterize Axl in metastatic melanoma.

Aim 2 Elucidate the mechanism for how Axl-Akt3 signaling affects metastasis in melanoma.

Aim 3 Validate whether the hypothesis model based on breast cancer (**Figure 3**) works in metastasis melanoma.

Materials

2.1 Materials for Cell culture

The 6 New Zealand Melanoma cell lines were generated from surgical samples of metastatic melanoma. Written consent was obtained from all patients under Auckland Area Health Board Ethics Committee guide lines [101, 102].

Table 1: Materials for Cell culture

Material	Supplier
MEM Alpha (1×)	Life technologies
FBS-HI (Fetal Bovine Serum)	Sigma
Transferrin	Sigma
Sodium Selenite	Sigma
Insulin	Sigma
Penicillin-Streptomycin	Sigma
Trypsin-EDTA solution	Sigma
PBS	Sigma
DMSO	Sigma

2.2 Materials for RT-PCR

Table 2: Materials for RT-PCR

Material	Supplier
Nuclease-free Water	Ambion by Life technologies
Glycogen	Ambion by Life technologies
Lithium chloride	Merck
Ethanol	Sigma
Axl primer	Applied Biosystems
Akt3 primer	Applied Biosystems
Human β-actin (20×)	Life technologies
Human 18S rRNA(20×)	Life technologies
LightCycle 480 Probes Master	Roche

Table 3: Kits for RT-PCR

Material	Supplier
RNeasy Mini Kit (50)	QIAGEN
High Capacity cDNA Reverse Transcription Kit	Applied Biosystems

2.3 Materials for Western blot

Table 4: Materials for protein isolation and measurement

Material	Supplier
NP40	Life technologies
Sodium dodecyl sulfate solution(SDS)	Sigma
Nadoc	Sigma
Trizma base	Sigma
Sodium chloride	Sigma
Aprotinin	Sigma
Leupeptin	Sigma
Natrium Vanadat	Sigma
PMSF	Merck
BCA protein assay kit	Thermo

Table 5: Materials for gel preparation

Material	Supplier
30% Acrylamide/Bis Solution	Bio-Rad Laboratories
Trizma base	Sigma
Sodium dodecyl sulfate solution(SDS)	Sigma
Ammonium persulfate	Sigma
TEMED	Sigma

Table 6: Materials for Western blot buffer

Material	Supplier
Trizma base	Sigma
Sodium chloride	Sigma
Sodium dodecyl sulfate solution(SDS)	Sigma
Glycine	Sigma
Tween-20	Sigma
Blotting-Grade Blocker	Bio-Rad Laboratories
Methanol	Sigma

Table 7: Materials for Western blot

Material	Supplier
Precision Plus Protein Standards	Bio-Rad Laboratories
Margic Mark XP Western Protein Standards	Life technologies
PVDF Transfer Membrane	GE Healthcare
Pierce ECL Western Blotting Substrate	Thermo

Table 8: Antibodies used for Western blot

Material	Supplier
Human Axl Antibody (AF154)	R&D systems
Anti-Akt3/PKBγ Antibody (05-780)	Merck Millipore
GAPDH (6C5) (sc-32233)	Santa Cruz Biotechnology
goat anti-mouse IgG-HRP (sc-2005)	Santa Cruz Biotechnology
donkey anti-goat IgG-HRP (sc-2056)	Santa Cruz Biotechnology
Phopho-Axl (Tyr702) (D12B2) Rabbit mAb	Cell signaling
HRP-Goat Anti-Rabbit IgG (H+L)	Invitrogen

2.4 Materials for xCelligence

Table 9: Materials for xCelligence

Material	Supplier
Matrigel	BD Biosciences
Trypsin Neutralizing Solution	Cell Applications, Inc
CIM-Plate 16	Roche
E-Plate VIEW 16	ACEA Biosciences

2.5 Materials for CRISPR

Table 10: Materials for CRISPR and Sequence

Material	Supplier
BG204: pSqCas9(BB)-2A-GFP	BerGenBio
Oligo 1: DL315 HsAxlEx7 afor	IDT
Oligo 2: DL316 HsAxlEx7 arev	IDT
Oligo 3: DL317 HsAxlEx7 bfor	IDT
Oligo 4: DL318 HsAxlEx7 brev	IDT
10× T4 Ligation Buffer	New England Biolabs
T4 Polynucleotide Kinase	New England Biolabs
10×FastDigest Buffer	Thermo Scientific
FastDigestBpil	Thermo Scientific
T7 DNA Ligase	New England Biolabs
C3019 (10-beta Competent E.coli)	New England Biolabs
LB medium	Sigma
LB Agar Tablets	Sigma
BigDye 3.1	Life technologies
5× Sequence Buffer	Life technologies
PBS,1× (without calcium and magnesium)	Cellgro
QIAprep Spin Miniprep Kit (50)	QIAGEN
Plasmid Midi Kit (100)	QIAGEN

Neon 10µl Kit	Invitrogen

2.6 Materials for Flow cytometry

Table 11: Antibodies and materials for flow cytometry

Material	Supplier
Formaldehyde Solution	Sigma
Bovine Serum Albumin	Sigma
Human Axl Antibody (AF154)	R&D systems
Alexa Fluor 647 donkey anti-goat IgG (H+L)	Life technologies

Methods

3.1 Cell culture

3.1.1 General maintenance

The six New Zealand melanoma (NZM) cell lines used for this study were generated from surgical samples of metastatic melanoma [103, 104]. Written consent was obtained from all patients under Auckland Area Health Board Ethics Committee guidelines. NZM cell lines were cultured in α-modified minimal essential medium supplemented with insulin (5 μg/ml), transferring (5 μg/ml), and sodium selenite (5ng/ml), 100 U/ml of penicillin, 100 μg/ml of streptomycin (PS), 5% fetal bovine serum (FBS). Instead of culture cells in incubators where the oxygen tension corresponds to atmospheric levels (21% O_2) like common practice work in vitroit was noteworthy that in this study the NZM cell lines were kept in a low oxygen incubator (5% O_2, 5% CO_2, 37 °C) in order to mimic physiologically low oxygen levels in tumors. Although it was not the usual way of culturing cells, but it was a key point in this study.

The NZM cells cultured in T75 flasks and were daily observed by microscope of Nikon ECLIPSE TS100. After installing a Nikon D3000 camera on this microscope and switching to photo format, the pictures were taken by Nikon D3000.

3.1.2 Cell thawing

Medium was pre-warmed in a 37°C water bath for 30 minutes. The cryovials containing NZM cells were removed from liquid nitrogen storage and were immediately placed into the 37°C water bath. When only a small bit of ice left, the vials were transferred into the flow hood. Before opening, the vials were wiped with 70% ethanol. The contents of each vial of cells were transferred to T-25 culture flasks containing 5 ml of medium, and then the flasks were put into a low oxygen incubator (5% O2, 5% CO2, 37 °C). The medium was changed with fresh medium after 4 hours. When cells reached about 80% confluence, which were transferred into T-75 flasks where cells were kept in culture.

3.1.3 Cell passaging

The cells were routinely passaged (every 2-3 days) after reaching approximately 70-90% confluency. Medium, 1×PBS and trypsin-EDTA were pre-warmed in 37°C water bath for 30 minutes before passaging. First, medium was removed, and cells were washed by 3 ml 1×PBS, then added 3 ml trypsin. After about 2-3 minutes incubating in incubator, the cells were observed under a light microscope. The side of flask was hit several times until cells were completely detached from substratum then 3 ml fresh medium was added to stop trypsin. The cell suspension was transferred into a 15ml tubes, and centrifuged at 1200 rpm for 5 minutes. The supernatant was removed and fresh medium was added. After suspending, cells were diluted 1:4 and transferred into new T-75 flask with 10ml fresh medium. The flasks were put back into low oxygen incubator.

3.1.4 Cell counting

Cell counting was performed by Millipore's Scepter handheld automated cell counter with 60μm sensors. Cells were harvested and suspend as described before, and transferred into a 1.5 mL Eppendorf tube. After the Scepter cell counter was turned on, and a 60μm sensor was attached to the end of the counter with the electrode sensing panel facing toward the front of the instrument. Because Scepter sensors consist of a precision molded sampling chamber, with an electronic sensing zone and integrated cell-sensing electrodes, it is possible to discriminate cell size at sub-micron resolution, and cell volume at sub-picoliter resolution. The plunger was depressed when it showed "Hold down the plunger to begin", then the sensor was submerged into the cell suspension solution and the plunger was released to aspirate the cell suspension into the sensor. When "Count Complete. Please remove sensor and discard." was displayed on the screen, the sensor was removed and the cell data was read.

3.1.5 Cell freezing

Cell lines in continuous culture are more easily to surfer genetic drift, senescence, microbial contamination and so on, so it is vitally important that they are frozen down and preserved for long-term storage. First, cells were washed, trypsinized, counted and centrifuged at 1200 rpm for 5 minutes when they are reached 70-90% confluence. Second the freezing medium was mix by 70% α-modified minimal essential medium, 20% FBS and 10% DMSO. Cells were resuspended in moderate freezing medium to create a cell concentration of 1×10^6 cells per ml. Then the cell freezing mixture was transferred into storage vials at 1 ml per cryovial. After labeled with name, passage number and date, cells were immediately transferred to -20°C for one hour, followed by -80°C overnight and then permanent storage in liquid nitrogen.

3.2 Analyzing Axl and Akt3 expression by RT-PCR

3.2.1 RNA isolation

RNA isolation was performed using RNeasy Mini Kit (50) according to the instruction. Cells for RNA extraction were cultured in 60mm dishes. When cells reached 70-90% confluence, it is ready for RNA isolation. First medium was aspirated completely, and cells were washed twice by PBS. Cells were disrupted by adding 600 µl RLT buffer, and then scraped and homogenized. After 600 µl of 70% ethanol was added, 700 µl well mixed lysate was transferred to RNeasy spin column which was placed in a 2 ml collection tube, then centrifuged at 10,000rpm for 15s, the flow-through was discarded. Secondly 700 µl buffer PW1 was added to the spin column and centrifuged as described above to wash the column membrane. After discarding the flow-through, 500 µl RPE buffer was added to the spin column, and centrifuged as above. Similarly the flow-through was discarded. Thirdly, 500 µl buffer RPE was added again, but centrifuged at 10,000 rpm for 2 minutes. After that, the RNeasy spin column was placed in a new 2 ml collection tube and centrifuged at full speed for 1 minute. Finally, the RNeasy spin column was transferred in a new 1.5 ml Eppendorf tube. After adding 30 µl of RNase-free water, it was centrifuged at 10,000rpm for 1 min to elute the RNA.

3.2.2 RNA precipitation

The RNA isolated from above was added with 1.5 µl Glycogen, 1.9 µl 8M Lithium chloride and 83.5 µl (2.5 volume) 100% ethanol, and then be frozen at -20 ºC overnight. The next day, it was spanned down for 30 min at full speed. After removing ethanol carefully, 500 µl of 70% ethanol was added and then it was spanned for 5 min at the same speed. Finally the ethanol was aspirated and the tube was dried in air for about 20 min. The RNA pellet was dissolved in 30 µl RNase-free waster, and measured by Nanodrop.

3.2.3 cDNA synthesis

cDNA making was performed using High Capacity cDNA Reverse Transcription Kit. Firstly 200 ng RNA sample was prepared in 10µl according to the concentration. Secondly 10 µl mastermix was mixed by adding 2µl 10× RT buffer, 0.8 µl 25× dNTP Mix 100mM, 2 µl 10× RT random primers , 1µl reverste tanscriptase and 4.2 µl RNase-free water. Thirdly 10 µl RNA sample and 10 µl mastermix were mix together and transferred in thermal cycler with the loading program 25ºC for 10min, 37ºC for 120min, 85ºC for 5min and 4º for holding. cDNA can be stored in -20ºC freezer.

3.2.4 RT-PCR

An optimal RT-PCR assay is absolutely essential for accurate and reproducible quantification of the samples. Therefore we first optimized our RT-PCR assay by performing serial dilutions of the templates and making standard curves. The primers and probes were validated for each target and the individual efficiencies were determined. In this part, Light Cycle 480 system was used to test gene expressing. The reaction (totally 10 µl) was mixed by 5µl Roche Mastermix, 2 µl RNase-free water, 0.5 µl reference probe including Human 18S rRNA(20×) or Human β-actin (20×), 0.5 µl Axl or Akt3 probe and cDNA template 2 µl. The cDNA template was diluted as 1:1, 1:10, 1:100, and 1:1000 in RNase-free water, and each sample was prepared four duplicates. The mixture was loaded in a 384 well plate and then transferred to Light Cycle 480 system with program as in **Table 12**. The crossing point (CP) value which was a cycle number in a log-linear region was used to calculate the quantitative value of RT-PCR. Based on the data, the standard curves were generated, and the amplification efficiencies of our samples were between 95%-105%.

After validation, we determined to use two reference genes, human beta-actin and human 18s RNA and evaluated at two concentrations 1:10 and 1:100. The reaction (totally 10 µl) was mixed as above: 5µl Roche Mastermix, 2 µl RNase-free water, 0.5 µl reference probe including Human 18S rRNA(20×) or Human β-actin (20×), 0.5 µl Axl or Akt3 probe and cDNA template 2 µl. Each sample was prepared three duplicates. The mixture was loaded in a 384 well plate and then transferred to Light Cycle 480 system with program as in **Table 12**. In quantitative analysis, we used the CP value of Axl or Akt3 to divide CP value of reference gene, then the data was collected and calculated for mean value, and the analysis figure was made based on the mean value with standard error by Excel 2010.

Table 12: Program setting of RT-PCR with Light Cycle 480 system

Thermal cycling conditions		
Stage	Temp. (ºC)	Time (mm:ss)
Pre-incubation	95	10:00
Amplification (45 cycles)		
Amplification-1	95	00:10
Amplification-2	60	00:30
Amplification-3	72	00:01
Cooling	40	00:30

3.3 Western blot

3.3.1 Preperation of the gel

The concentration of gel is determined by aim protein size. According to the size of our aim protein including Axl (140 kDa) and Akt3 (56 kDa), 10% SDS-PAGE gel was chosen as separating gel, and 4% as stacking gel. Firstly glass plates were cleaned and dried, after fixing the glass plates well water was filled between the plates and standed for 30 min to check whether it was clogged. Secondly ingredients were mixed as **Table 13** except 10% ammonium persulfate and TEMED, for they need to be added in just before. After 30 min water was removed and the plates were dried by filter paper if it didn't leak. At this time, the last ingredients, 10% ammonium persulfate and TEMED, were added and mixed with other ingredients then added between layers. After 30-45 min gel was stiff then added stacking gel. Stacking gel making was the same with separating gel, and the materials form was **Table 14**. Gel could be kept in running buffer (stated below) in 4ºC for about one month.

Table 13: 10% separating gel making solutions

10% Separating gel (1.5mm)	
30% Acrylamide/Bis Solution	3.33ml
1.5M Tris ph8.8	2.5ml
MilliQ H2O	4ml
10% SDS	100µl
10% ammonium persulfat	50µl
TEMED	5µl

Table 14: 4% Separating Gel making solutions

4% Separating gel (1.5mm)	
30% Acrylamide/Bis Solution	670µl
0.5M Tris ph6.8	1.25ml
MilliQ H2O	3ml
10% SDS	50µl
10% ammonium persulfat	50µl
TEMED	5µl

3.3.2 Protein isolation

In this part, we chose NP-40 RIPA buffer as lysis buffer, it was made as **Table 15-16**.

Table 15: NP-40 Ripa buffer making solutions

Solution	Composition	Volume
NP40	1%	10ml
10% SDS	0.1%	10ml
Nadoc	0.5%	5g
1M Tris ph7.4	50mM	50ml
5M Nacl	150mM	30ml
H2O		868ml
Total		1L

Table 16: RIPA lysis buffer making solutions

Solution	Composition
Aprotinin (1µg/µl)	1µl
Leupeptin (1µg/µl)	1µl
Natrium Vanadat 100el 200mM	10µl
PMSF 100mM	10µl
NP-40 RIPA Lysis buffer	978µl
Total	1ml

Cells for protein isolation were cultured in T75 Flask until they reached 70-90% confluency. Medium was removed and the cells were washed by PBS. 500 µl of RIPA buffer were added. After 1-2 min cells were scraped and transferred to a 1.5 Eppendorf tube. It was centrifuged at full speed for 5 min at 4 °C. Final the lysate was transferred to a new Eppendorf tube and prepared for measurement. The protein sample could be stored at -20 °C.

3.3.3 Western blot buffers

In Western blot, different kinds of buffer were needed including running buffer, transfer buffer, washing buffer and blocking buffer. All the buffers were made as following forms (**Table 17-20**):

Table 17: Running buffer making solutions

Running buffer 10× 1L	
Solution	Composition
Tris (Mw=121.14)	30.3g
Glysine (Mw=75.07)	144g
20% SDS	10g(50ml)
MilliQ H_2O	1L
Running buffer 1× 1L	
Running buffer 10×	100ml
MilliQ H_2O	900ml

Table 18: Transfer buffer solutions (store at 4°C)

Transfer buffer 10× 1L	
Solution	Composition
Tris (Mw=121.14)	30.3g
Glysine (Mw=75.07)	144g
MilliQ H_2O	1L
Transfer buffer 1× 2L	
Transfer buffer 10×	200ml
100% Methanol	400ml
MilliQ H_2O	1400ml

Table 19: Washing buffer solutions

Washing buffer TBS 20× 2L (PH 7.6)	
Solution	Composition
Tris (Mw=121.14)	96.8g
NaCl	320g
MilliQ H_2O	1.5L (adjust PH with HCl)
Washing buffer TBST 1× 1L	
Washing buffer TBS 20×	50ml
Tween-20	1ml
MilliQ H_2O	950ml

Table 20: Blocking buffer solutions

Blocking buffer	
Solution	Composition
Marvel Milk powder	2.5g
Washing buffer TBST 1×	50ml

3.3.4 Western blot

According to the concentration of protein samples, each sample was contained 20 µg protein, sample loading buffer 8.75 µl and MilliQ H_2O until the total reached 35 µl. All the samples were mixed well and boiled at 90 °C for 5 min. Marker was mixed with 3.5 µl Magic marker and 8 µl protein standard. After loading sample into the wells of SDS-PAGE gels, the gels electrophoresis ran at 90V for about 70 min. When protein separation was down, transfer sandwiches were made by sponges, filter paper, gel and Nitrocellulose membrane activated with Methanol. The cassettes were placed in tankers with ice, and ran at 100V for 60min. After transferring the membranes were blocked in blocking buffer for 60 min. Antibodies Human Axl Antibody (1 µg/ml), Anti-Akt3/PKBγ Antibody (1:1000) and Phospho-Axl (Tyr702) Antibody (1:1000) were diluted in 1× TBST, and the membranes were incubated in antibodies at 4 °C overnight.

The membranes were washed by TBST 4×5 min, and incubated with 2° antibodies for 90 min at room temperature. After washing as before, the membranes were transferred into Super Signal West Femto Maximum Sensitivity Substrate (mixed 1:1) and were ready for imaging. The images were acquired by ChemiDoc™ XRS+ System with Image Lab™ Software. After that, membranes were incubated with the GAPDH antibody at 4°C overnight, and then 2° antibody and imaged as above. Then images were analyzed by software of Image Lab 3.0.

In quantitative analysis, after aim bands were found and adjusted, the sum of all intensities within the band boundaries showed with Volume (Int) value was calculated by quantitative tools in the software. Then the Int value of Axl , phosphor-Axl or Akt3 in each cell lines was divided by the Int value of GAPDH correspondingly, and the expression analysis figures were made based on these data with standard error by Excel 2010.

3.4 xCelligence

3.4.1 Principle of xCelligence

In our study, cell function test experiments were all performed with the xCelligence system, which is an electronic real-time cell-sensing assay (RTCA), providing real-time, continuous sensitive monitoring of cellular responses [105]. The RTCA instrument is composed of a RTCA impedance analyzer, a computer with RTCA software for controlling the system operation, electronic microwell plates and the RTCA station which is placed inside the tissue culture incubator. The microwell plates such as E-Plate and CIM-Plate whose bottoms are 80% covered with microelectrodes that measure the impedance differences within an electrical circuit. These differences are converted into cell index (CI), a value that may be influenced by several parameters, such as cell number, cell size, cell-substrate, or cell–cell attachment which also directly influenced by cell attachment, spreading, and/or cell proliferation. Featuring a dual-plate (DP) format, the instrument measures impedance-based signals in both cellular and cell invasion/migration (CIM) assays – without the use of exogenous labels. With outstanding application flexibility, the RTCA DP Instrument supports multiple users performing short-term and long-term experiments.

3.4.2 Cell Proliferation analysis by xCelligence

For cell proliferation analysis, the E-Plate was used in this xCelligence system. And the cell proliferation assay were performed twice, at the first time RTCA station was placed in a normal incubator (37°C, CO_2 5%, O_2 21%), at the second time RTCA station was placed in a low oxygen incubator (37°C, CO_2 5%, O_2 5%).

100 µl of cell culture medium was added to each well for the impedance background measurement. The cells of six NZM cell lines were harvest as before, and were added as **Table 21**. After adding the cells, the final volume was 200 µL. The E-Plates were monitored on the RTCA system at 200 sweeps×30 minutes for up to 100 hours. **Table 21: The layout of E-Plate for cell proliferation**

A1: NZM9 (20000 cells)	A2: NZM9 (20000 cells)
B1: NZM17 (20000 cells)	B2: NZM17 (20000 cells)
C1: NZM22 (20000 cells)	C2: NZM22 (20000 cells)
D1: NZM40 (20000 cells)	D2: NZM40 (20000 cells)
E1: NZM59 (20000 cells)	E2: NZM59 (20000 cells)
F1: NZM86 (20000 cells)	F2: NZM86 (20000 cells)
G1: Control (only medium)	G2: Control (only medium)
H1: Control (only medium)	H2: Control (only medium)

3.4.3 Cell Migration analysis by xCelligence

The ability of cell migration was also monitored in real-time with the xCelligence system (CIM-Plates), also both with the normal incubator (37°C, CO2 5%, O2 21%) and a low oxygen incubator (37°C, CO2 5%, O2 5%).The CIM-Plate is composed of two chambers, only the bottom of lower chamber has microelectrodes. In the migration assay 5% Fetal Bovine Serum (FBS) in the lower chamber was as attractant. The lower chamber was added 160 µl medium (**Table 22**), and the upper chamber was added 30 µl Serum-free medium. After assembling the CIM-Plate, it was performed for background measurement. The cells of the six NZM cell lines were washed and trypsinized. TNS solution was added at a 1:1 ratio to stop trypsinization. After centrifuging as before, cells were resuspended in FBS-free medium and then seeded in the upper chamber **Table 22**. The CIM-plates was left in an incubator for 30 minutes to allow cell attachment. The impedance value of each well was automatically monitored by the xCelligence system at 100 sweeps×15 minutes for 25h and expressed as a CI value.

Table 22: The layout of CIM-Plate for cell migration

A1: upper-NZM9 (20000 cells) in FBS free medium, lower-5%FBS medium	A2: upper-NZM9 (20000 cells) in FBS free medium, lower-5%FBS medium
B1: upper-NZM17(20000 cells) in FBS free medium, lower-5%FBS medium	B2: upper-NZM17(20000 cells) in FBS free medium, lower-5%FBS medium
C1: upper-NZM22(20000 cells) in FBS free medium, lower-5%FBS medium	C2: upper-NZM22(20000 cells) in FBS free medium, lower-5%FBS medium
D1: upper-NZM40(20000 cells) in FBS free medium, lower-5%FBS medium	D2: upper-NZM40(20000 cells) in FBS free medium, lower-5%FBS medium
E1: upper-NZM59(20000 cells) in FBS free medium, lower-5%FBS medium	E2: upper-NZM59(20000 cells) in FBS free medium, lower-5%FBS medium
F1: upper-NZM86(20000 cells) in FBS free medium, lower-5%FBS medium	F2: upper-NZM86(20000 cells) in FBS free medium, lower-5%FBS medium
G1: upper-FBS free medium, low-FBS medium	G2: upper-FBS free medium, low-FBS medium
H1: upper- FBS free medium, low-FBS medium	H2: upper- FBS free medium, low-FBS medium

3.4.4 Cell Invasion analysis by xCelligence

Detection of cell invasion was performed with the xCelligence system RTCA DP Instrument and CIM-Plate using Matrigel basement membrane matrix. Matrigel is a meshwork of extracellular matrix (ECM) proteins and growth factors which mimics the basement membrane underlying epithelial cells and has been broadly used for assessing cell invasion, especially cancer cell invasion in vitro. Firstly the upper chamber of CIM-Plate was coated with 20 µl of Matrigel which was diluted at 1:20 with serum free medium and left in 37°C incubator for 4 hours. Each well in the lower chamber was filled with 160 µl as **Table 23**. After 1 hour 37°C incubation, the CIM-Plate 16 was performed a background measurement.

Table 23: Arrangement of Matrigel and medium in CIM-Plate 16 for cell invasion

A1: upper-Matrigel 1:20 pre-coated, lower-160 µl of 5% FBS medium	A2: upper-Matrigel 1:20 pre-coated, lower-160 µl of 5% FBS medium
B1: upper-Matrigel 1:20 pre-coated, lower-160 µl of 5% FBS medium	B2: upper-Matrigel 1:20 pre-coated, lower-160 µl of 5% FBS medium
C1: upper-Matrigel 1:20 pre-coated, lower-160 µl of 5% FBS medium	C2: upper-Matrigel 1:20 pre-coated, lower-160 µl of 5% FBS medium
D1: upper-Matrigel 1:20 pre-coated, lower-160 µl of 5% FBS medium	D2: upper-Matrigel 1:20 pre-coated, lower-160 µl of 5% FBS medium
E1: upper-Matrigel 1:20 pre-coated, lower-160 µl of 5% FBS medium	E2: upper-Matrigel 1:20 pre-coated, lower-160 µl of 5% FBS medium
F1: upper-Matrigel 1:20 pre-coated, lower-160 µl of 5% FBS medium	F2: : upper-Matrigel 1:20 pre-coated, lower-160 µl of 5% FBS medium
G1: upper-Uncoated, lower-160 µl of 5% FBS medium	G2: upper-Uncoated, lower-160 µl of 5% FBS medium
H1: upper-Uncoated, lower-160 µl of FBS free medium	H2: upper-Uncoated, lower-160 µl of FBS free medium

Cells of the six NZM cell lines were harvest as cell migration part, and seeded as **Table 23**.The CIM-plates was left in an incubator for 30 minutes to allow cell attachment. The impedance value of each well was automatically monitored by the xCelligence system at 100 sweeps×15 minutes for 25h and expressed as a CI value.

3.5 CRISPR

3.5.1 Principle of CRISPR

Clustered regularly interspaced palindromic repeats (CRISPR) is a microbial nuclease system which consists of the CRISPR-associated (Cas) genes and noncoding RNA elements, can program the specificity of nucleic acid cleavage. Type II CRISPR/Cas9 uses a CRISPR RNA (crRNA) and a trans-activating RNA (tracrRNA) to guide the Cas9 DNA endonuclease to induce sequence-specific double-strand breaks (DSBs) [106, 107]. CRISPR/Cas9 mediated DSBs of the target DNA is recognized and repaired by the cellular DNA repair machinery via non-homologous end joining (NHEJ) typically resulting in short nucleotide deletions or insertions (indels), which disrupt the target gene [108] or homology-directed repair (HDR), which can be exploited to precisely edit genomic sequence or insert exogenous DNA [109].

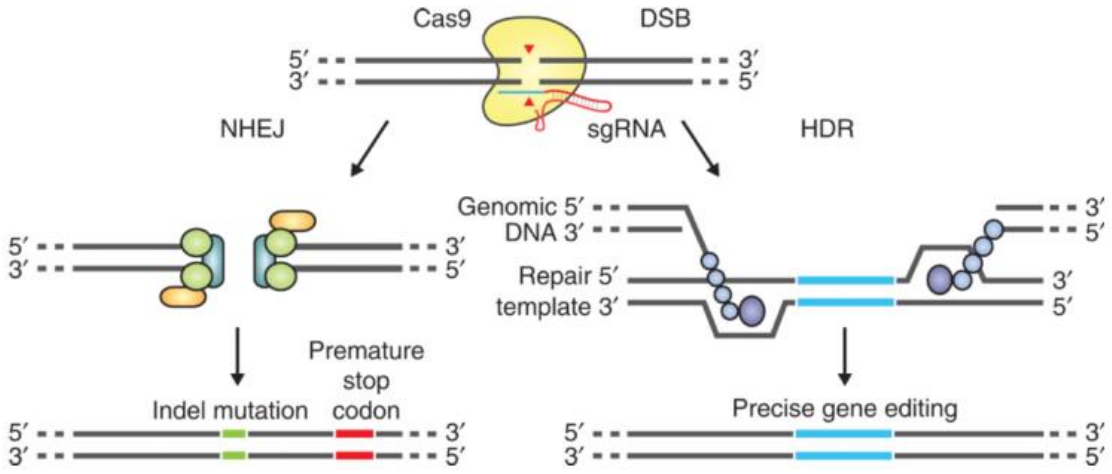

Figure 4: DSBs can be repaired via NHEJ or HDR. In the error-prone NHEJ pathway, it can result in random indel mutations at the site of junction. Indel mutations occurring within the coding region of a gene can result in frameshifts and the creation of a premature stop codon, resulting in gene knockout. Alternatively, a repair template in the form of a plasmid or ssODN can be supplied to leverage the HDR pathway, which allows high fidelity and precise editing. Adapted from Reference [110].

3.5.2 Target selection of Human Axl

Human Axl genomic DNA sequence was inputed in an online CRISPR Design Tool (NCBI), the 20-bp sequence directly upstream of any 5′ -NGG was identified. According to NCBI Gene, there may be a human Axl splice form that used alternative 5' exons. One place to make gRNA would be to the first COMMON exon, which is exon 7, and another place to make gRNA would be to kinase domain. In this study, Hs Axl exon 7 was chosen as the target sequence. And according to the target sequence, two pairs of oligos were ordered from IDT Company.

3.5.3 Making of CRISPR construct

In this part, two pairs of oligos were resuspended to a final concentration of 100 μM. The mixture was made (**Table 24**) for phosphorylating and annealing the oligos. The mixture was placed in a thermocycler by using the following parameters: 37 °C for 30 min; 95 °C for 5 min; ramp down to 25 °C at 5 °C min–1. Then the annealed oligo was diluted 1:250 by adding 1 μl of oligo to 249 μl of room temperature ddH_2O.

Table 24: Reaction solutions for making CRISPR construct.

Component	Amount (μl)
Oligo 1: Hs Axl for (100 μM)	1
Oligo 2: Hs Axl rev (100 μM)	1
T4 ligation buffer, 10×	1
T4 PNK	0.5
ddH2O	6.5
Total	10

When the oligos was phosphorylated and annealed, they were cloned into pSpCas9n(BB)-2A-GFP(PX461) which contains marker GFP to aid the selection of transfected cells.A ligation reaction was set up as described below **Table 25**. The ligation reaction was then incubated in a thermocycler: 37^{o}C 5 min, 23^{o}C 5 min, cycle the previous two steps for 6 cycles (total run time 1h), 4 ^{o}C hold until ready to proceed.

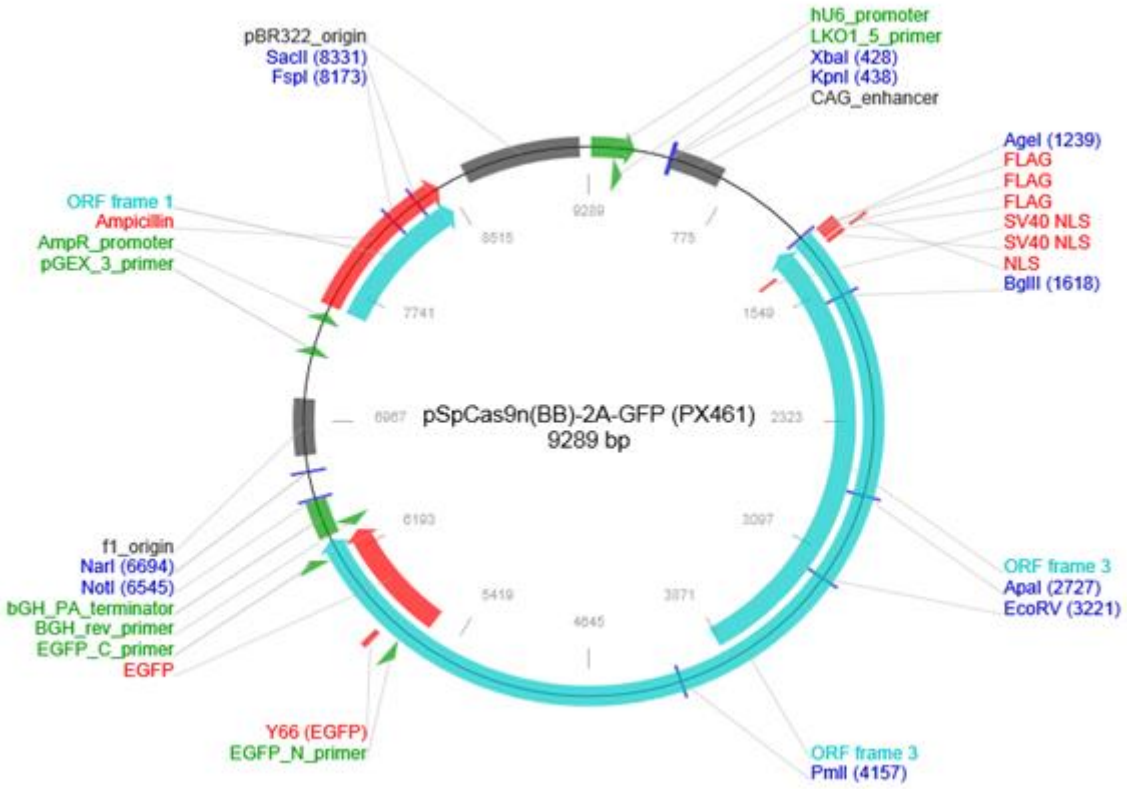

Figure 5: Gene map of pSpCas9n(BB)-2A-GFP(pX461). It carries a GFP marker for identification of transfected cells.

Table 25: Reaction solutions for ligation reaction

Component	Amount (µl)
pSpCas9(BB), 100 ng (13.25ng/µl)	7.5
phosphorylated and annealed oligo duplex from above (1:250 dilution)	2
FastDigest Buffer, 10×	2
DTT (10mM to a final concentration of 1mM)	1
ATP (10mM to a final concentration of 1mM)	1
FastDigest BbsI	1
T7 DNA ligase	0.5
ddH2O	5
Total	20

3.5.4 Transform the plasmid into NEB 10-beta competent E.coli (C3019).

According to the protocol supplied with the cells, cells were thawed on ice and 50µl of cells was mixed and transferred into a transformation tube. Then 5 µl of CRISPR construct was added into the transformation tube, the mixture was incubated on ice for 30 min, heated-shock at 42 °C for 30 s, returned immediately to ice for 5 min. 950 µl of room temperature SOC medium was added into the mixture, which was then placed at 37°C for 60 min. After performing several 10-fold serial dilutions (1:10, 1:100, and 1:1000) in SOC, 100 µl of each dilution were spread onto the pre-warmed selection plates containing ampicillin 100 µg/ml. The plates were incubated at 37°C for 24 hours.

3.5.5 DNA isolation for sequencing

From each plate, 2 colonies were picked to check for correct insertion of gRNA. Each single colony was inoculated into a 10 ml LB medium with 100 µg/ml ampicillin by sterile pipette tips. Then it was cultured and shaken at 37 °C overnight. The isolation of the plasmid DNA from cultures was performed using a QIAprep spin miniprep kit according to the manufacturer's instructions.

10 ml bacterial overnight culture was centrifuged at 10,000 rpm for 3 min at room temperature, and then the cells were resuspended in 250 µl P1 buffer and transferred into Eppendorf tubes. After adding 250 µl P2 buffer, tubes were mixed thoroughly, then the same as 350 µl N3 buffer. Tubes were centrifuged at 13,000 rpm for 10 min, and the supernatant was transferred into QIAprep spin column for 45s centrifuging. After adding 500 µl buffer PB, they were centrifuged as before, so did 750 µl buffer PE. Finally residual washing buffer was removed by 1 min centrifuging, and DNA was eluted by adding 50 µl buffer EB which was measured by Nanodrop.

Table 26: A mixture reaction was made for sequencing.

Component	Amount
BigDye v3.1	1 µl
Sequence buffer, 5x	2 µl
DK157 primer, 10µM	0.5
DNA templat	200ng
MilliQ	-
Total	10 µl

Table 27: The program for mixture reaction in a thermocycler

Temperature	Time	Cycles
96 °C	1 min	1
96 °C	10 sec	25
50 °C	5 sec	
60 °C	4 min	
4 °C	hold	-

After got the concentration of DNA from Nanodrop, the volum of 200 ng DNA in each sample was calculated. Then the materials in **Table 26** was mixed and followed by a reaction as **Table 27** in a thermocyler. After reaction, DNA was sent for sequencing, which was performed by Sekvenseringslaboratoriet (under Seksjon for laboratoriediagnostikk ved Senter for medisinsk genetikk og molekylærmedisin, Haukeland Universitetssykehus).

3.5.6 DNA isolation for transfection

This part was similar with DNA isolation with QIAprep spin miniprep kit described above, which was performed using a QIAGEN Plasmid Midi Kit according to the manufacturer's instructions. This protocol was designed for preparation of up to 100 µg of high- or low-copy plasmid or cosmid DNA. The colony which has right sequence results was picked and inoculated into a 150 ml LB medium with 100 µg/ml ampicillin by sterile pipette tips. Then it was cultured and shaken at 37 °C overnight.

The bacterial cells were harvested by centrifugation at 6000 ×g for 15 min at 4 °C, and then resuspended in 4 ml buffer P1. After adding 4 ml buffer P2, it was mixed thoroughly and incubated at room temperature for 5 min. 4 ml buffer P3 was added and mixed, incubated on ice for 15 min. Tubes were centrifuged at 20,000 rpm for 30 min at 4°C, and the supernatant was transferred and continued centrifuging at 20,000 rpm for 15 min at 4°C. A QIAGEN-tip 100 was equilibrated by adding 4 ml buffer QBT, the column was allowed to empty by gravity flow, it was repeated with the supernatant from centrifugation. The QIAGEN-tip was washed twice by 10 ml buffer QC. Then the DNA was eluted by 5 ml buffer QF which was also measured by Nanodrop.

3.5.7 Transfection

Electroporation is one of the most efficient non-viral methods for transferring exogenous DNA into mammalian cells. In this part, we used Neon transfection system to transfect the DNA described above to our NZM17 cells. The Neon system employs specialized consumable pipette tips containing gold-plated electrodes as electroporation chamber, and has three electric parameters including Pulse voltage, Pulse width and Pulse number, In general, the use of such a capillary electroporation system (which is often called a microporation device) has important advantages compared with conventional cuvette-based electroporation chambers including high efficiency, flexibility, simplicity, versatility and easy to use protocol.

Microporation was done using the Neon™ Transfection System as follows: NZM17 cells were split when they reached 70%-90% confluent, the next day medium was changed with medium without antibiotics. On the third day, NZM17 cells were washed with PBS (without Ca^{2+} and Mg^{2+}) and trypsinized for exactly 3 min at 37 °C, and the detached cells were counted and centrifuged in non-antibiotics medium at 400×g for 5 min. The cell pellet was resuspended, and 2.5×10^5 cells were transferred to a tube and again centrifuged. We added 25 µg CRISPR DNA plus 250 µl R-buffer to the pellet (0.5-2 µg DNA/10µl mixture/well). 10 µl of the volume of this mixture was aspirated into the Gold-Tip of the MicroPorator Pipette of the Neon™ Transfection System. After microporation as followed Optimization (**Table 28)**, the 10 µl inside the Gold-Tip was immediately released into a 24-well plate already filled

with culture medium without antibiotics—this step was repeated with the other 230 µl of the above-mentioned mixture. Then the 24-well plates were placed into the low oxygen incubator (37°C, 5%CO_2, 5%O_2). Culture medium with antibiotics was changed 24 hours later, and the plate was ready for Fluorescent picturing. After finding the best transfection condition, the transfection was repeated under the best condition setting.

Table 28: Optimization form

Sample	Well no.	Pulse voltage	Pulse width	Pulse no.
1	A1	0 (control)	0 (control)	0 (control)
2	A2	1400	20	1
3	A3	1500	20	1
4	A4	1600	20	1
5	A5	1700	20	1
6	A6	1100	30	1
7	B1	1200	30	1
8	B2	1300	30	1
9	B3	1400	30	1
10	B4	1000	40	1
11	B5	1100	40	1
12	B6	1200	40	1
13	C1	1100	20	2
14	C2	1200	20	2
15	C3	1300	20	2
16	C4	1400	20	2
17	C5	850	30	2
18	C6	950	30	2
19	D1	1050	30	2
20	D2	1150	30	2
21	D3	1300	10	3
22	D4	1400	10	3
23	D5	1500	10	3
24	D6	1600	10	3

3.5.8 Brightfield and Fluorescence microscopy

After transfection, the NZM17 cells cultured in 24-well plates were monitored daily using an Olympus CKX41 inverted fluorescence microscope connected to a power supply unit U-RFLT50. The Olympus CKX41 has blue (Fluorescein isothiocyanate, FITC) filters and is suitable for regular cell observation including GFP and other fluorescence applications. Post-transfection fluorescence images of NZM17 cells were acquired by Nikon TE2000 system. The Nikon TE2000 system was composed of TE2000 inverted microscope, mercury/UV lamp, NIS-Elements software (NIS-Elements AR 4.20.00), TE2000 control pad, color camera, and so on. After the system was switched on, the post-transfection NZM17 cells in a well of a 24-well plate were focused in the TE2000 inverted microscope. A camera control unit of DS-U2/L2 USB was selected in NIS-Elements AR 4.20.00 software, and the correction collar in the objectives was adjusted for cover slip thickness between 0 and 2mm. In the lambda window, the optical configurations of brightfield and FITC were selected. Then the pictures were taken separately under brightfield and FITC filters. After photographing, three kinds of cells pictures can be acquired including a mono picture, a FITC picture and a coincide picture. The fluorescence microscopy was repeated with each well of every 24-well plates with post-transfection NZM17 cells.

3.6 Flow cytometry

3.6.1 Principle of flow cytometry

Flow cytometry is defined as the simultaneous measurement of multiple physical characteristics of a single cell as the cell flows in suspension through a measuring device. It is a subset of the field of cytometry based on the use of specialized instruments. In flow cytometry, the measurements are made as the cells or particles pass through the measuring apparatus. A flow cytometer includes a laser beam used as the light source to excite a fluorescent tag bound to the cells in the specimen; an argon laser which produces light; a cell sorter, or flow sorter, which uses electrical and/or mechanical means to divert and collect cells (or other small particles) with measured characteristics that fall within a user-selected range of values and so on.

Flow cytometry measures multiple characteristics of individual particles flowing in single file in a stream of fluid. Light scattering at different angles can distinguish differences in size and internal complexity, whereas light emitted from fluorescently labeled antibodies can identify a wide array of cell surface and cytoplasmic antigens. This approach makes flow cytometry a powerful tool for detailed analysis of complex populations in a short period of time [111].

3.6.2 Protocol

In this part, we used flow cytometry to check the expression of Axl after CRISPR knocking out. In the first time, NZM17 cells which were cultured 72 hours post transfection were collected by washing with PBS, trypsinization and centrifugation at 1200 rpm/5 min. Then the cells were resuspended in PBS, counted and the concentration was adjusted to 10^6cells/ml. 2 ml sample and negative control of NZM17 cells without transfection were directly sent for sorting GFP positive cells by flow cytometor FACS Aria (performed by Marianne Enger).

After sorting, cells were cultured in a T75 flask as before. When cells were enriched, the post sorting NZM17 cells were collected by washing with PBS, trypsinization and centrifugation at 1200 rpm/5 min. Then the cells were resuspended in 100 µl formaldehyde mixed with 900 µl PBS (final concentration 4%) and fixated for 10 min at 37ºC. After 1 more min on ice, the cells were resuspended in PBS and the concentration was adjusted to 10^6cells/ml.

3 Eppendorf tubes were prepared and labelled, and each was added 1 x 106cells. After adding 1 ml PBS-1% BSA to each tube, the tubes were centrifuge at 700×g for 5 min. The most of supernatant was gently aspirated, and the cells were resuspend by gently tapping the tube. 100 µl of diluted anti-Axl in cold PBS-1%BSA was added to the third tube (final concentration is 2.5 µg/106 cells), the other two tubes were added only 100 µl of PBS-1%BSA, and all of the three tubes were incubated for 30 min at room temperature in tublewheel. After incubation all the tubes were washed with 1 ml PBS-1%BSA and centrifuged above twice. 100 µl of diluted secondary antibody Alexa Fluor® 647 (final concentration 10µg/ml) was added to the second and third tube; 100 µl of PBS-1% BSA was added to the first tube. Like above, these were mixed well and kept in tublewheel at room temperature for 20 minutes. Then it was also followed by washing with PBS-0.5% BSA and centrifuging twice. Finally, cells were resuspended in 250 µl PBS-0.5% BSA. Data was acquired by using a flow cytometer Acurri C6, and analyzed by cFlow Sampler Analysis software.

In the second time, NZM17 cells which were cultured 24hour, 48hours, and 72 hours after transfection were tested Axl and GFP expression by flow cytometer Acurri C6 as above without sorting.

3.7 Statistical analysis

In this study, all the statistics analysis was performed by Excel 2010. The data in expression experiments was first calculated for ratio by dividing reference contrast, and then expressed with mean ± SD ($\bar{x}\pm s$). Column figures were based on the mean value and showed error bars with standard error. In cell function analysis, the data in figures were also based on mean value of two replicates and showed with SD.

Results

4.1 Expression analysis of NZM cell lines

4.1.1 Morphology of NZM cell lines

We received six NZM cell lines from New Zealand; they were thawed and cultured in a low oxygen incubator (5% O_2, 5% CO_2, 37°C). In common practice for in vitro cell culture, cells were often cultured in normal incubators (5% CO_2, 37°C) where the O_2 tension corresponds to atmospheric levels (21% O_2) [112]. However, the endogenous physiological O_2 tension found in tissues was in the range of 2–5% [113, 114], in order to mimic physiologically low oxygen levels in tumors, the six NZM cell lines were cultured in the low oxygen incubator (5% O_2, 5% CO_2, 37°C). The morphology of the cell lines varied, with some being more epithelial-like and others more fibroblastic-like (**Figure 6**). When cells reached 70-90% confluence, they were 1:4 passaged. However, the requiring passing time was different: NZM17, NZM40, and NZM86 required passaging 2 times a week, while NZM9, NZM22 and NZM59 required passaging 1 time a week.

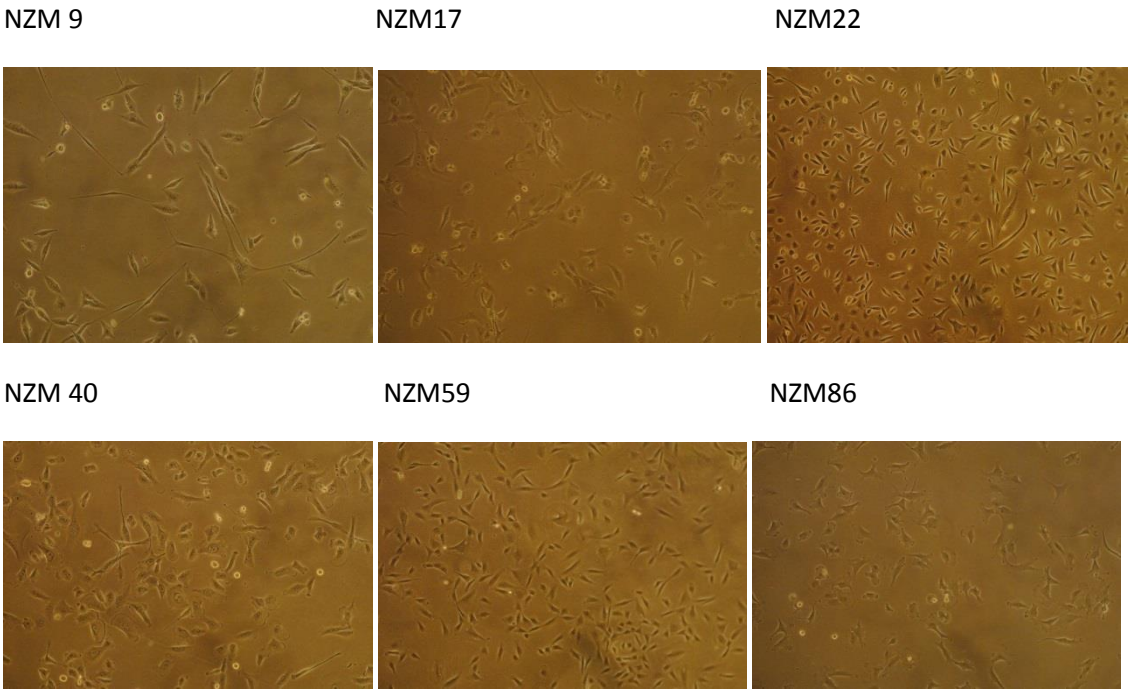

Figure 6: Images of the six NZM cell lines (100× under microscope of Nikon ECLIPSE TS100). The morphology of the cell lines varies: NZM9 was more fibroblastic-like and others more epithelial -like.

4.1.2 Expression of Axl in the NZM cell lines.

According to Kim et al., all the six cell lines expressed high level of Axl [115]**.** In order to validate the Axl expression level in our six NZM cell lines, we measured the Axl expression both in gene level by RT-PCR and protein level by Western blot. The data was shown in **Figure 7** and **Figure 8**. In RT-PCR, we used two reference genes, human beta-actin and human 18s RNA, besides we also evaluated at two concentrations:1:10 and 1:100. According to the Crossing Point (CP) value of the six NZM cell lines, we used Axl CP value to divide CP value of reference gene, and organized the data shown in **Figure 7**. From **Figure 7**, we can find that when human beta-actin is used as reference gene, the difference expression level of Axl was comparably obvious. From the CP definition, a higher of CP value means the lower expression. From this analysis, NZM17 had the highest expression of Axl, besides NZM40 and NZM86 expressed relatively lower Axl.

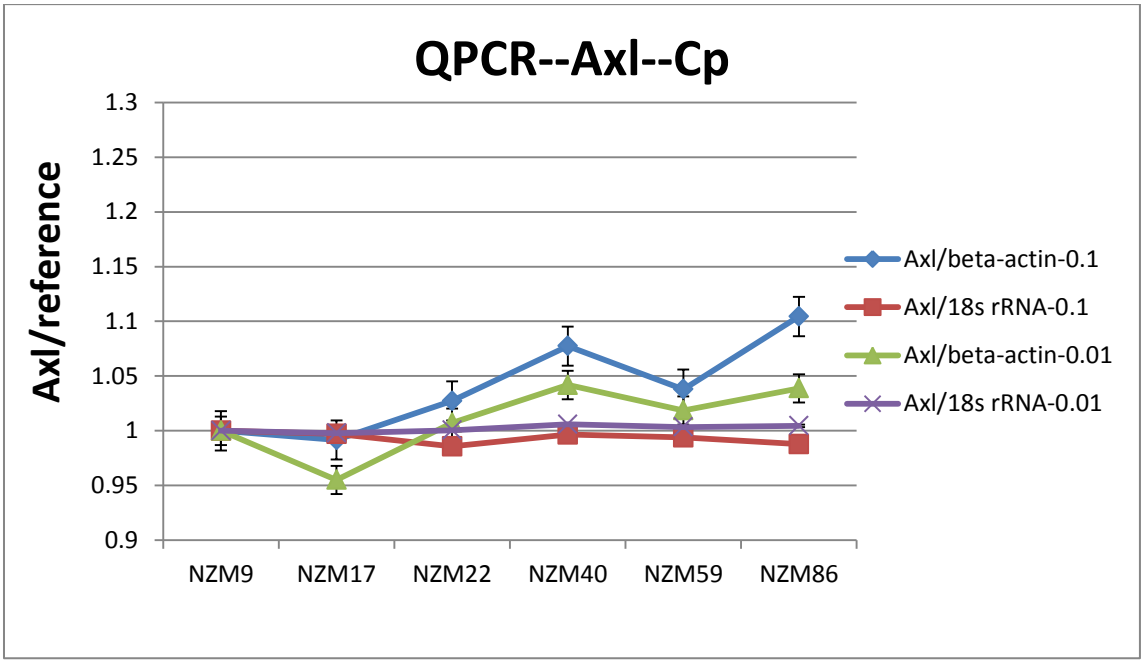

Figure 7: CP value of Axl as ratios to two reference genes including human beta-actin and human 18s rRNA at two concentration levels (1:10, 1:100).

To further check Axl expression among the six NZM cell lines at protein level, and also to validate the data from Kim [115], we did Western blot to analyze the Axl and phospho-Axl expression among them. The data was shown in **Figure 8A**, we also quantificed the Western blot results, shown in **Figure 8B**. From both **A** and **B**, we can find that NZM17 has the highest expression of Axl, corresponding with the RT-PCR results, while the other cell lines have quite low expression or even do not express Axl protein. Our results differ with the data from Kim et al. [115]**.** According to Kim et al., all of the six NZM cell lines have similar high signal of Axl, but in our data (**Figure 8A**) only NZM17 has quite strong signal, NZM9 and NZM22 have relatively high signals, while the other three do not show clear bands; and according to Kim et al., NZM9, NZM17 and NZM86 all have relatively high ratios as to reference β-actin, but in **Figure 8B** only NZM17 has obviously high ratio as to reference GAPDH compared with others.

A

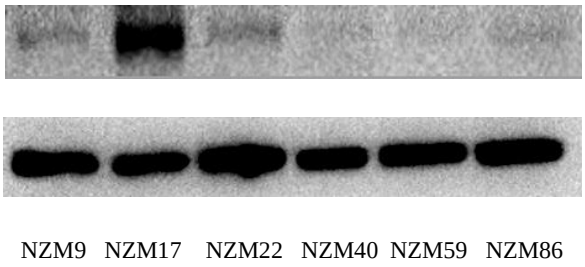

B

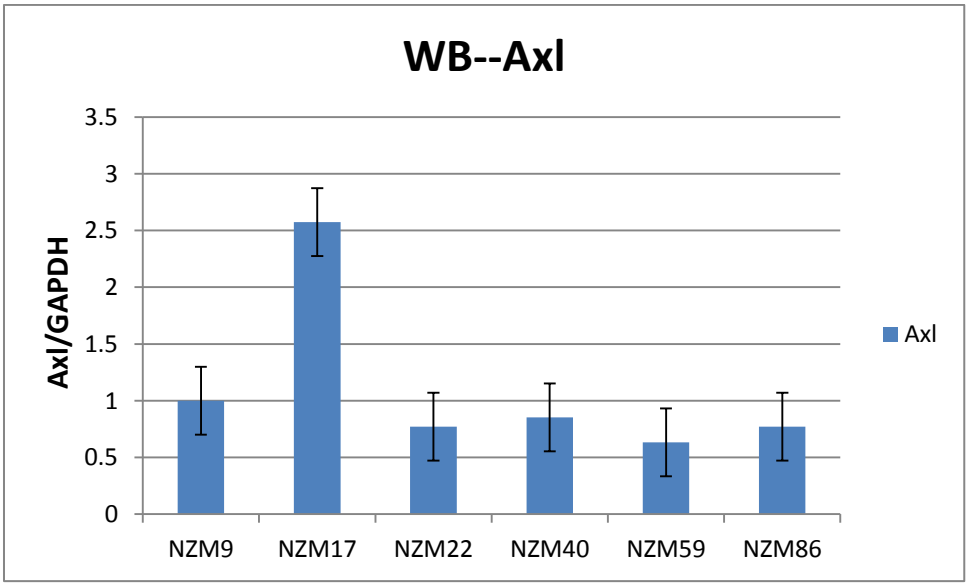

Figure 8: Western results of Axl in the six NZM cell lines with GAPDH as reference. A shows the bands of Axl and GAPDH of the six NZM cell lines, in which NZM17 has the strongest signal band in Axl expression; B shows the quantification results of Western blot.

We also analyzed the level of phospho-Axl (Y702) to measure Axl activation levels among the six NZM cell lines. The data was shown in **Figure 9**. The quantitation (**Figure 9B**), shows that NZM17 had the highest level of phospho-Axl.

A

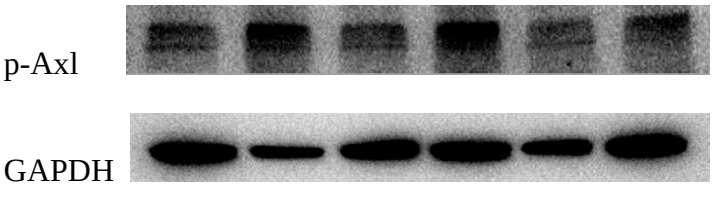

B

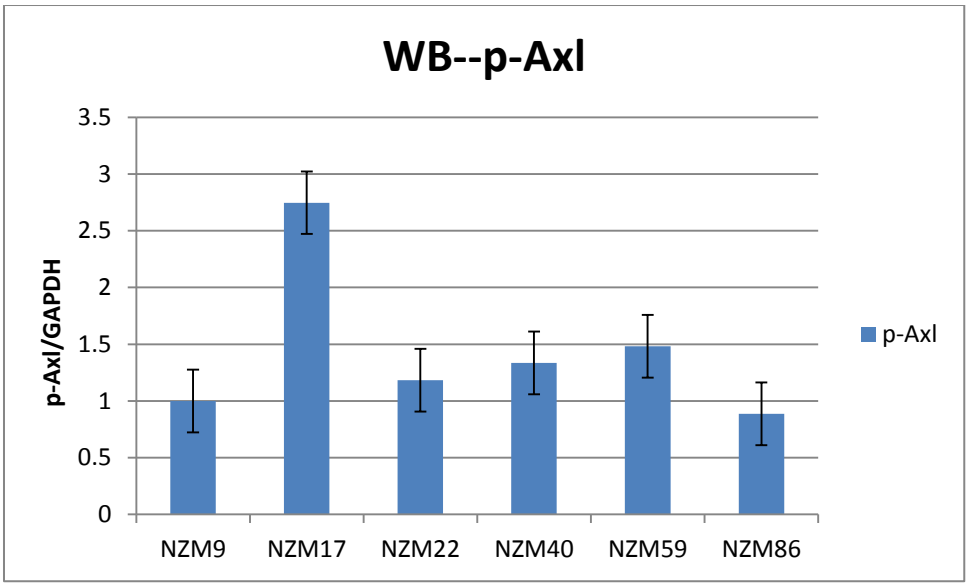

Figure 9: Western results of pAxl (Y702) in the six NZM cell lines with GAPDH as reference. A shows the bands of pAxl and GAPDH of the six NZM cell lines, in which NZM17 has the strongest signal band in pAxl expression; B shows the quantification results of western blot.

4.1.3 Expression of Akt3 in the six NZM cell lines.

To test the hypothesis model of Axl affect melanoma metastasis via activation of Akt3, Akt3 expression analysis perfomed at transcript level by RT-PCR and protein level by Western blot. First, we used RT-PCR to find whether all the six cell lines express Akt3, the data was shown in **Figure 10**. Similar with Axl expression of RT-PCR, we also checked the Akt3 expression with two reference gene human beta-actin and human 18s RNA in two concentration levels 1:10 and 1:100. From **Figure 10** we can see that even using different reference genes and concentrations, we got similar CP value trends. NZM40 had the highest CP value suggesting the lowest Akt3 mRNA expression. Also in **Figure 10,** it showed NZM17, NZM22 and NZM86 had relatively higher CP value indicating a relatively low Akt3 expression. NZM9 and NZM59 had higher expression of Akt3.

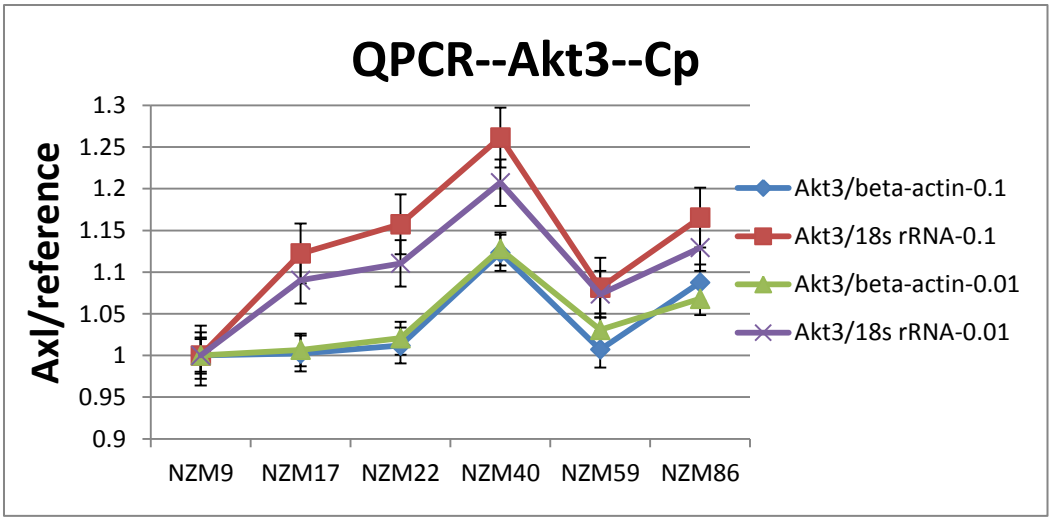

Figure 10: CP value of Akt3 as ratios to two reference genes including human beta-actin and human 18s rRNA at two concentration levels (1:10, 1:100).

We also checked the Akt3 protein expression levels by Western blot. The data is shown in **Figure 11**. Different with the gene expression results from RT-PCR (**Figure 10**), we found that NZM86 has the highest expression of Akt3 (**Figure 11**). Besides we found that NZM9 has the lowest expression of Akt3 (**Figure 11B**), which was opposite to the results in RT-PCR (**Figure 10**, in which NZM9 has the lowest CP value with the highest expression gene level of Akt3).

A

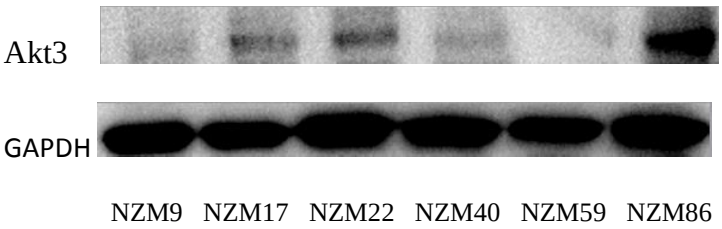

B

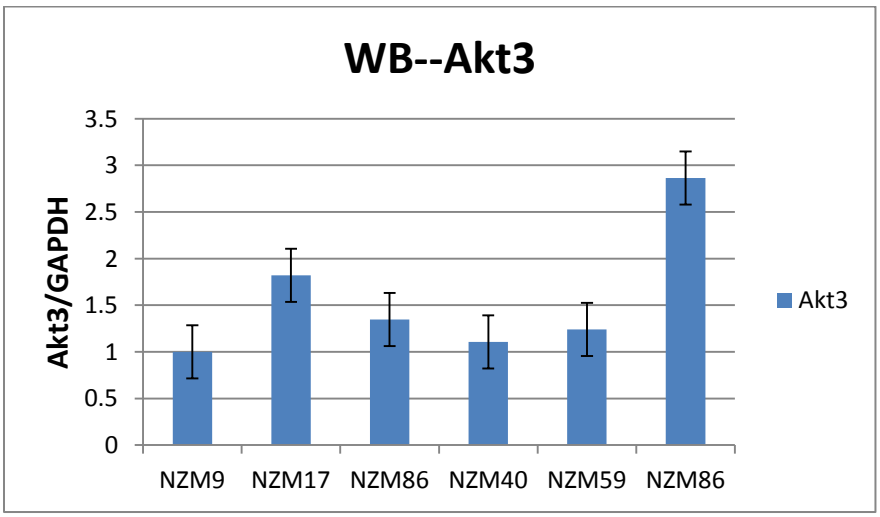

Figure 11: Western blot results of Akt3 in the six NZM cell lines with GAPDH as reference. A shows the bands of Akt3 and GAPDH of the six NZM cell lines, in which NZM86 has the strongest signal band in Akt3 expression; B shows the quantification results of Western blot.

4.2 Cell function analysis of the six NZM cell lines by xCelligence system

4.2.1 Proliferation

We tested the proliferation of our six NZM cell lines by xCelligence system, we did it twice separately in a normal incubator (21% O_2, 5% CO_2, 37ºC) and a low oxygen incubator (5% O_2, 5% CO_2, 37ºC).The figure of growth from xCelligence system was shown in **Figure 12A** (21% O_2) and **B** (5% O_2). Firstly we found cells grew differently when the oxygen concentration was different. **Figure 12A** showed that NZM17 which was an Axl-Akt3 co-expression cell line had the highest CI value, but it needed the longest time to arrive stable. Besides NZM40 and NZM86 had comparatively higher proliferation level while NZM9, NZM22 and NZM59 have lower level. **Figure 12B** showed similar comparison results among the six cell lines. However CI value of NZM17 and NZM22 showed a clear reduction around 40 hours later before they arrived stable.

To study the difference of cell proliferation between the two incubators with different oxygen concentration, we compared the CI value from two incubators at three time points including 24, 48 and 100 hours. The data was shown in **Figure 12C, D,** and **E**. From **Figure 12C** we can find that the Axl-Akt3 co-expression NZM17 grew faster in the low oxygen incubator than the normal incubator at 24 hours, but the growth rate of NZM17 in low oxygen incubator reduced over time (**Figure 12D**). From **Figure 12E** we found the CI value of low oxygen incubator became lower than normal incubator. Besides we can also find that NZM40 grows faster in normal incubator and NZM59 grew faster in low oxygen incubator.

A

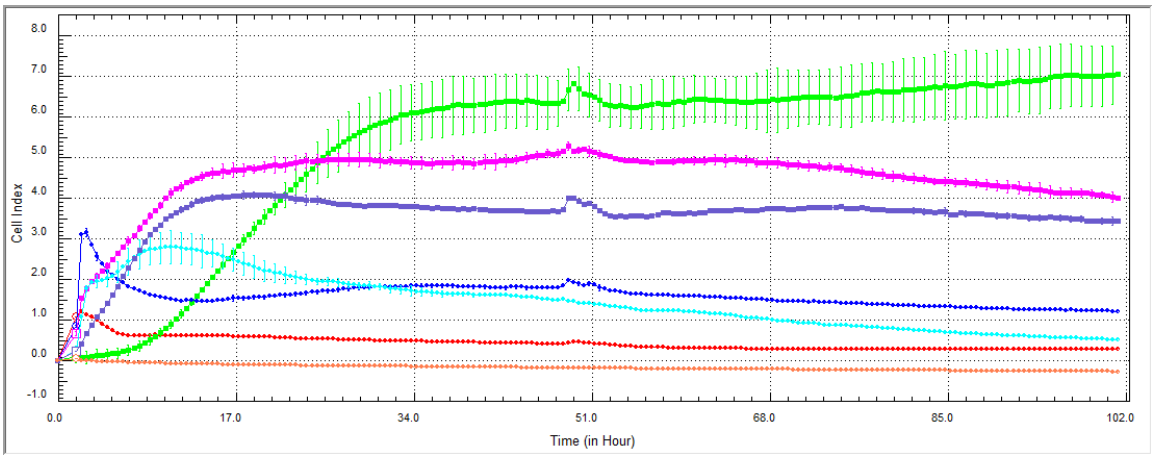
Cell Index
Time (in Hour)

B

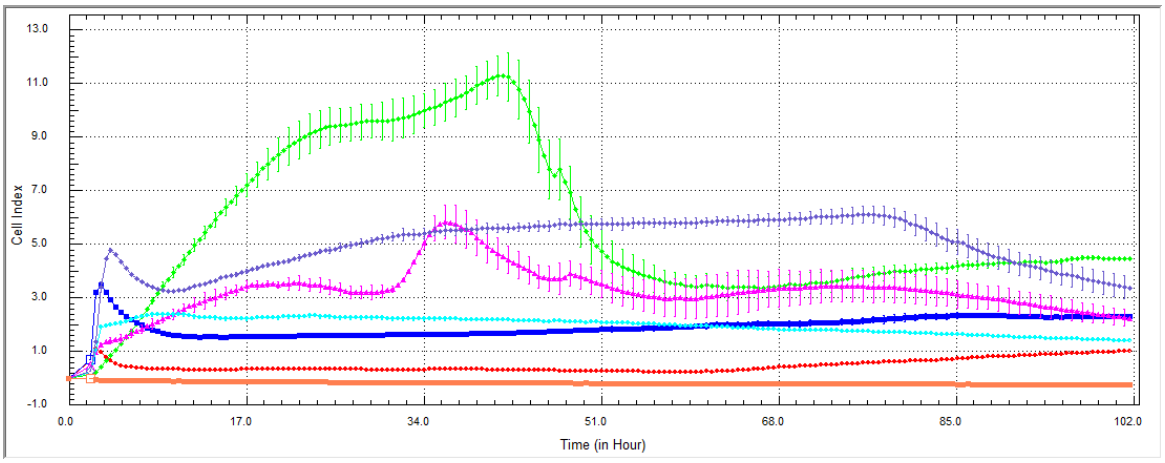
Cell Index
Time (in Hour)
RED
GREEN
BLUE
MAGENTA
CYAN
SLATEBLUE
NZM9
NZM17
NZM22
NZM40
NZM59
NZM86

C

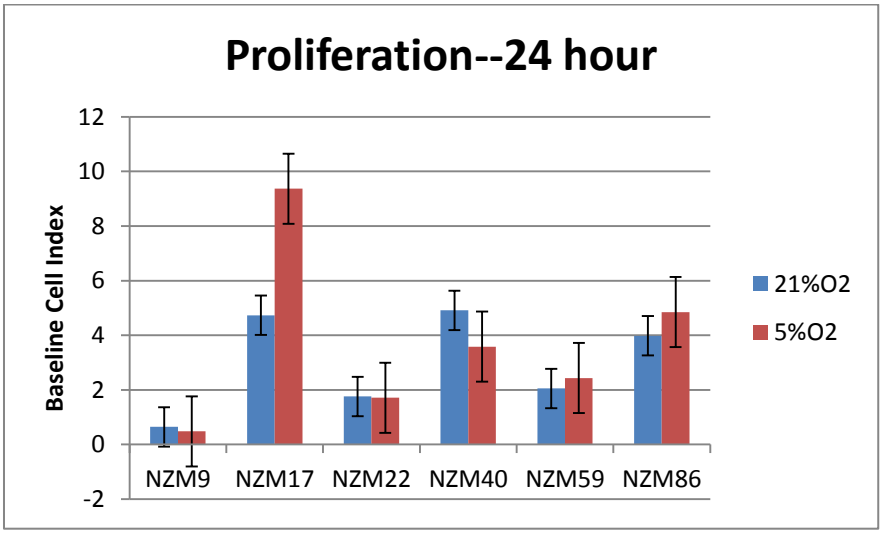
Proliferation--24 hour
Baseline Cell Index
21%O2
5%O2
NZM9
NZM17
NZM22
NZM40
NZM59
NZM86

D

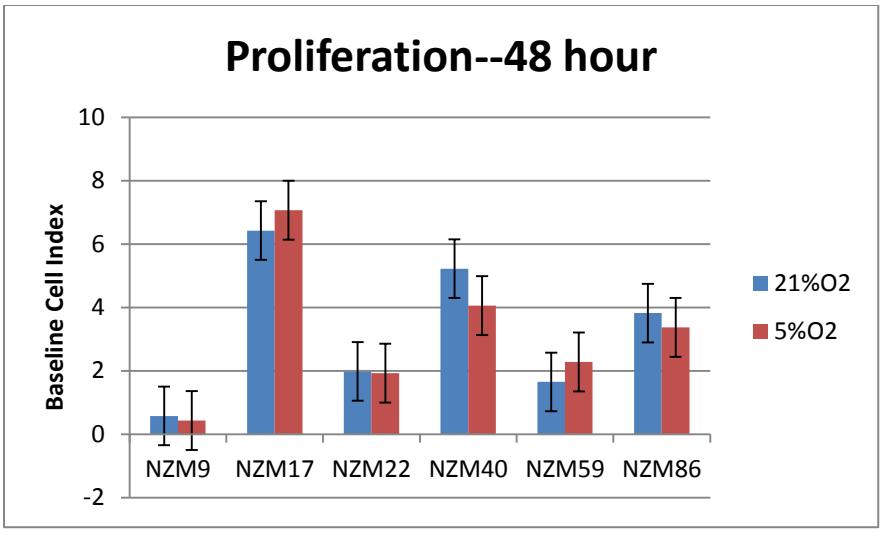

E

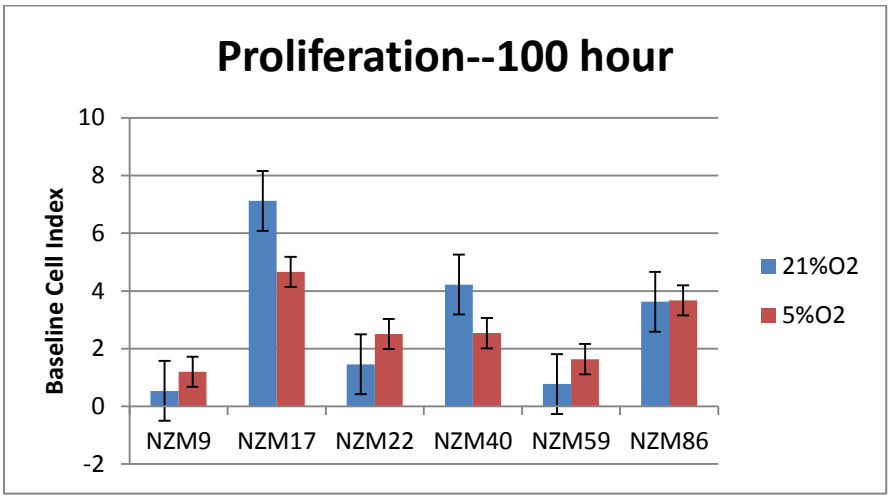

Figure 12: The different proliferation level of the six NZM cell lines tested by xCelligence system. A: Proliferation tested by xCelligence in a normal incubator (21% O_2. 5% CO_2, 37°C); B: Proliferation tested by xCelligence in a low oxygen incubator (5% O_2. 5% CO_2, 37°C); C: CI value comparison at 24 hour; D: CI value comparison at 48 hour; E: CI value comparison at 100 hour.

4.2.2 Migration

Similar to proliferation experiment, the migration experiment was also performed by xCelligence system separately in two oxygen concentration incubators (**Figure 13**). From **Figure 13A** and **B**, we found that all the CI trend lines of the six NZM cell lines were quite similar; the only difference was in NZM40, but the Standard deviation (SD) of it was quite bigger in both **Figures 13A** and **B**, so we cannot prove the weather the migration level was different in different oxygen concentration incubators. We also compared the CI value from two incubators (**Figure 13C**), it was shown that there was no big differences expect NZM40, which was coincide the results from **Figure 13A** and **B**. The Axl-Akt3 co-expression cell line NZM17 also showed much higher cell migration compared with other cell lines.

A

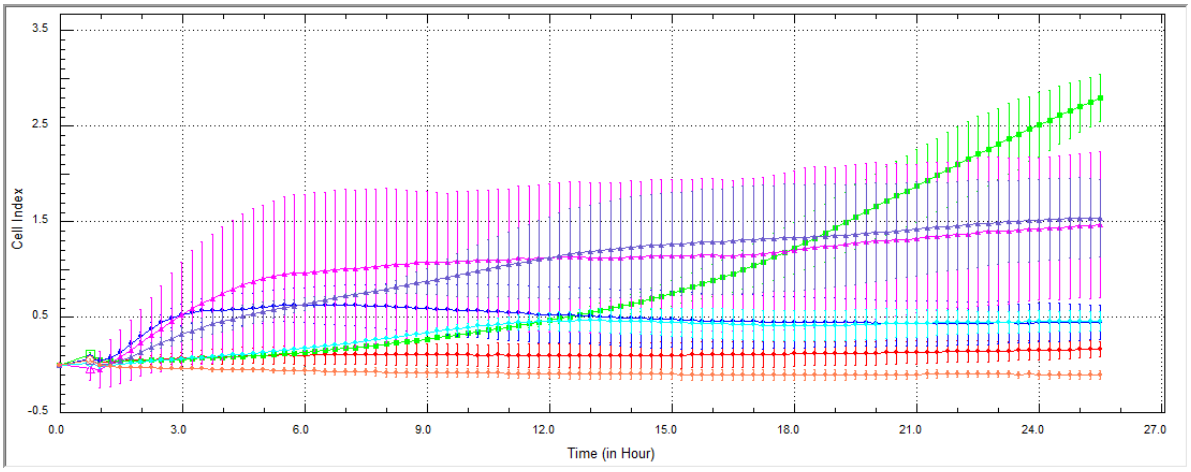

B

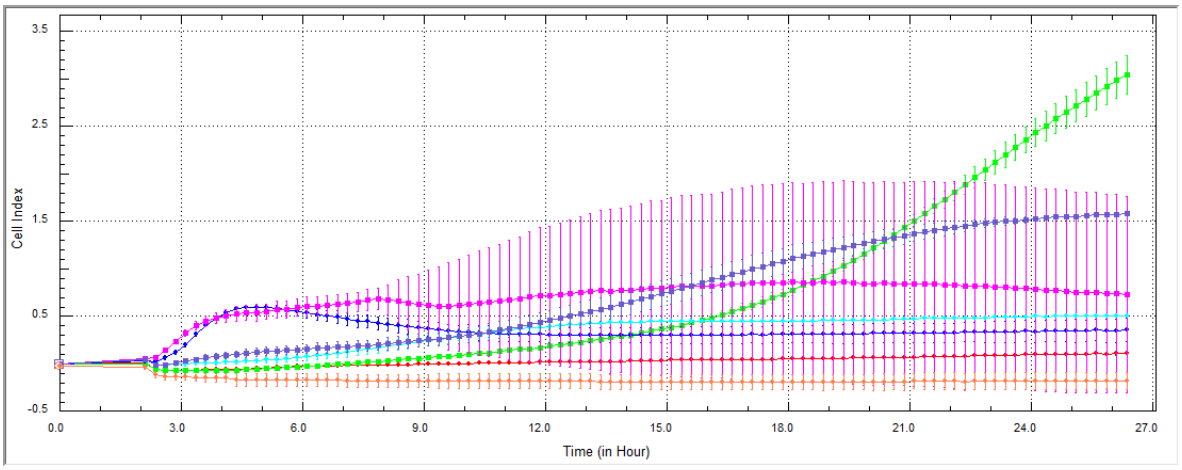

NZM9 NZM17 NZM22 NZM40 NZM59 NZM86

C

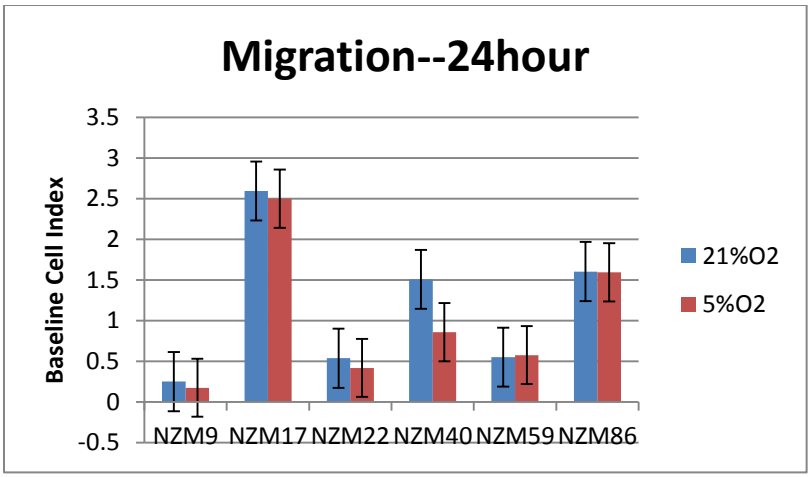

Figure 13: The migration level of the six NZM cell lines tested by xCelligence system. A: Migration tested by xCelligence in a normal incubator (21% O_2. 5% CO_2, 37°C); B: Migration tested by xCelligence in a low oxygen incubator (5% O_2. 5% CO_2, 37°C); C: CI value comparison at 24 hour.

4.2.3 Invasion

Figure 14 showed the data of Cell Invasion experiment by xCelligence system performed in the two kinds of incubator. It was obviously different oxygen concentration had an important influence in cell invasion ability. In **Figure 14A**, the CI value of NZM9, 17 and 59 improved a lot after 20 hours, while the other three cell lines still kept relatively lower and stable CI value. In **Figure 14B**, NZM40 which had the highest CP value of Akt3 (**Figure 10**) showed the highest invasion level; and NZM86 which had the highest Akt3 expression in protein level (**Figure 11A** and **B**) had the lowest CI value of invasion. Besides, the Axl-Akt3 co-expression cell line NZM17 showed relatively higher invasion level both in normal incubator and low oxygen incubator. According to the results of comparison in **Figure 14C**, it was obvious that most NZM cell lines showed higher invasion ability in normal incubator than the low oxygen incubator expect NZM22.

A

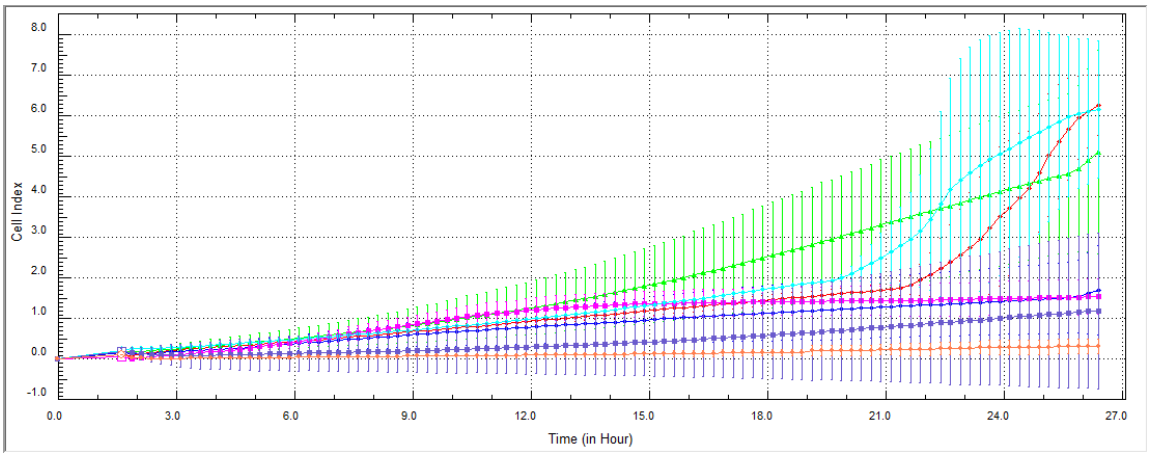

B

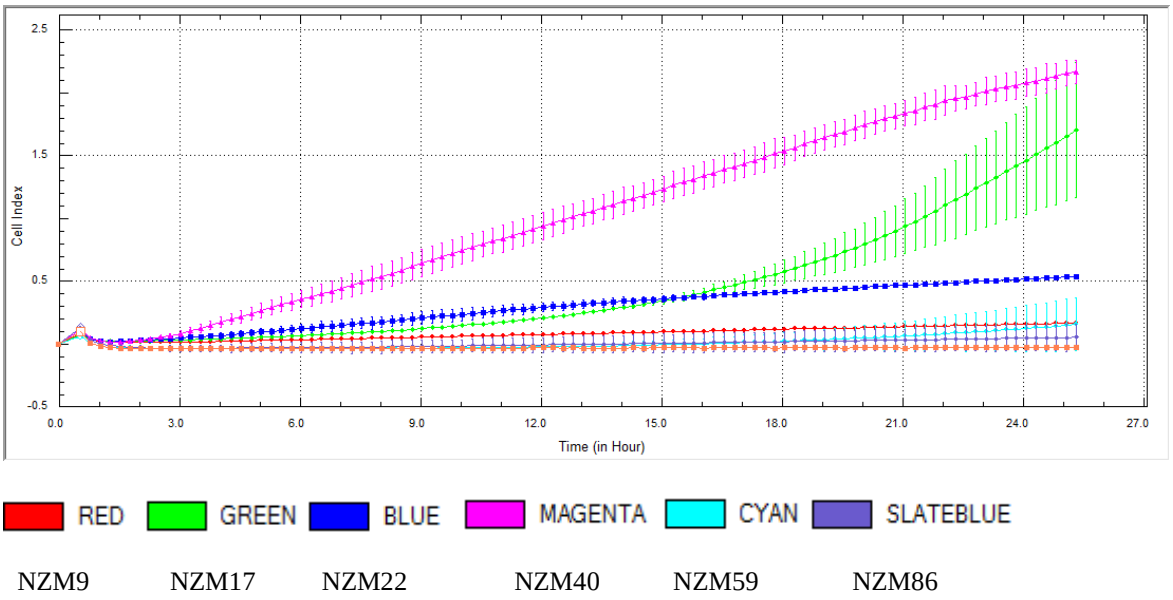

C

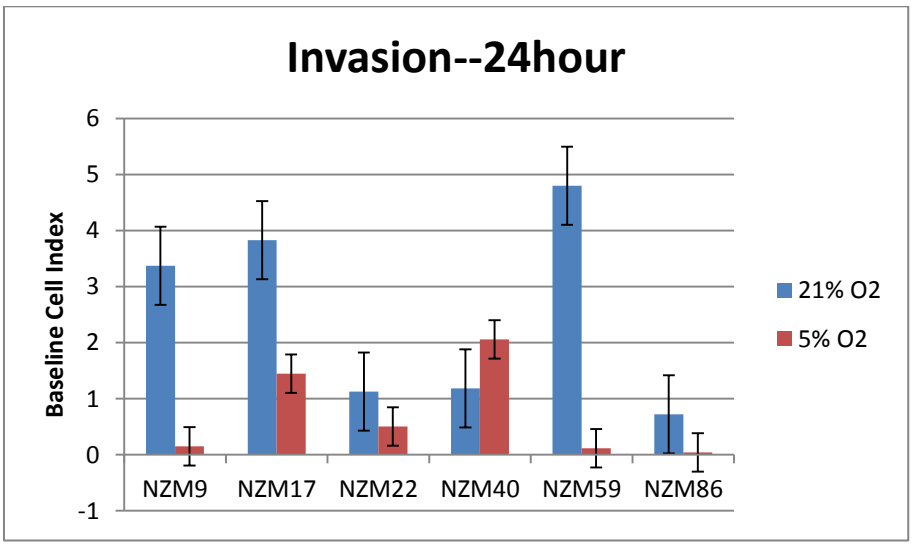

Figure 14: The Invasion level of the six NZM cell lines tested by xCelligence system. A: Invasion tested by xCelligence in a normal incubator (21% O_2. 5% CO_2, 37°C); B: Invasion tested by xCelligence in a low oxygen incubator (5% O_2. 5% CO_2, 37°C); C: CI value comparison at 24 hour.

4.3 Axl knocking out by CRISPR

CRISPR is a microbial nuclease system which consists of the CRISPR-associated (Cas) genes and noncoding RNA elements, can program the specificity of nucleic acid cleavage. CRISPR/Cas9 mediated DSBs of the target DNA is recognized and repaired by the cellular DNA repair machinery via NHEJ which can disrupt the target gene [108] or HDR, which can be exploited to precisely edit genomic sequence or insert exogenous DNA [109]. Therefore, we may permanently knock out Axl by using this system.

4.3.1 Target selection of Human Axl

The target selection of Human Axl was done by Dr. David Micklem. Human Axl genomic DNA sequence was inputted in an online CRISPR Design Tool (NCBI), the 20-bp sequence directly upstream of any 5′ -NGG was identified. According to NCBI Gene (**Figure 15**), Hs Axl exon 7 was chosen as the target sequence, and two pairs of oligos were ordered accordingly. The oligos was phosphorylated, annealed, and cloned into pSpCas9n(BB)-2A-GFP(pX461) which contains marker GFP to aid the selection of transfected cells. Then the CRISPR construct were enriched by NEB 10-beta competent E.coli and clonies were formed in selection plates.

Hs Axl Exon 7:

Top scoring pair from MIT (no off targets) is:

Guide A	87
quality	high
cuts after position	166 in query
sequence	GCTGCCTAGCCGAAGCTGATggg
# offtargets	92
# genic offtargets	21

Guide B	97
Quality	high
cuts after position	217 in query
sequence	CACCCCTTATCACATCCGCGtgg
# offtargets	35
# genic offtargets	4

Oligos to order for Hs Axl Exon7:

GuideAfor	caccGCTGCCTAGCCGAAGCTGAT
GuideArev	aaacATCAGCTTCGGCTAGGCAGC
GuideBfor	caccgCACCCCTTATCACATCCGCG
GuideBrev	aaacCGCGGATGTGATAAGGGGTGc

Figure 15: Design and order oligos. For Axl, exon 7 was chosen to make gRNA. According to the top scoring, two guide sequences were chosen and two pairs of oligos were ordered. (with Dr. David Micklem).

4.3.2 Sequence of CRISPR constract

After the CRISPR construct prepared, we sequenced 6 clones from different dilution selection plates. The expected insertion of gRNAs sequence was detected in 5 clones and one of the clones did not show the right sequence (**Figure 16**). **Figure 16A** and **B** showed that the sequence Guide A forward oligo (highlighted in red box) was successfully cloned into the plasmid; **Figure 16D, E** and **F** showed that the sequence of Guide B forward oligo (highlighted in red box) were seamlessly cloned into the plasmid; in **Figure 16C**, we did not find the right insertion.

A

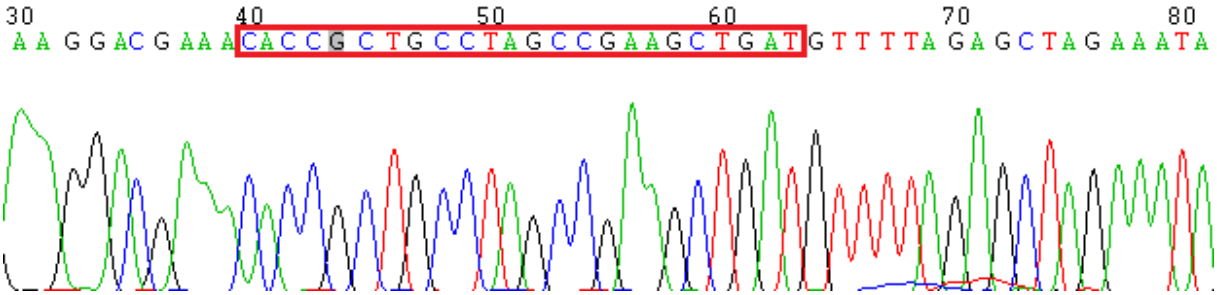

B

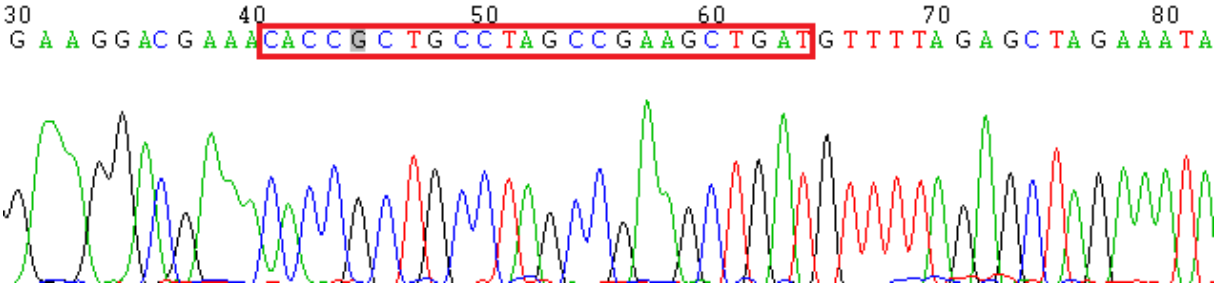

C

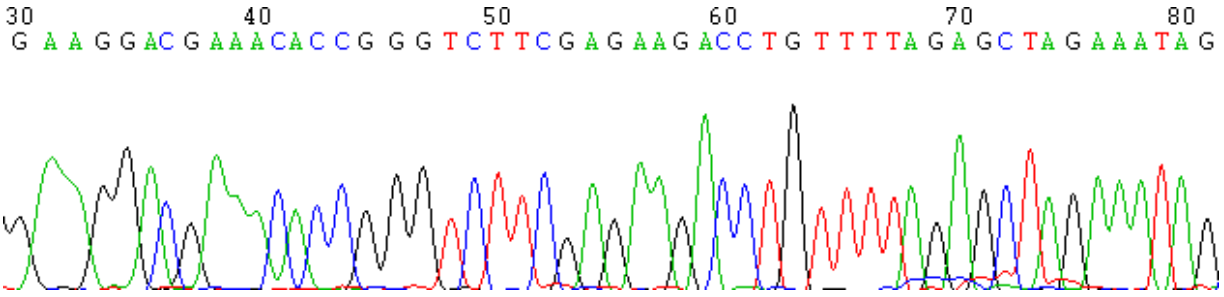

D

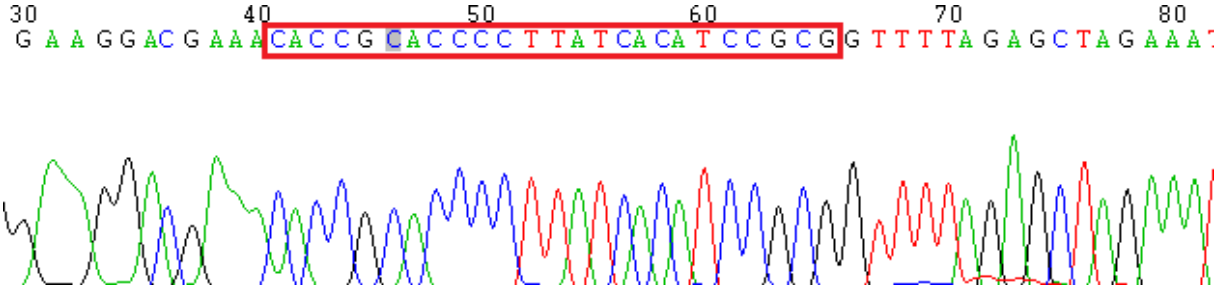

E

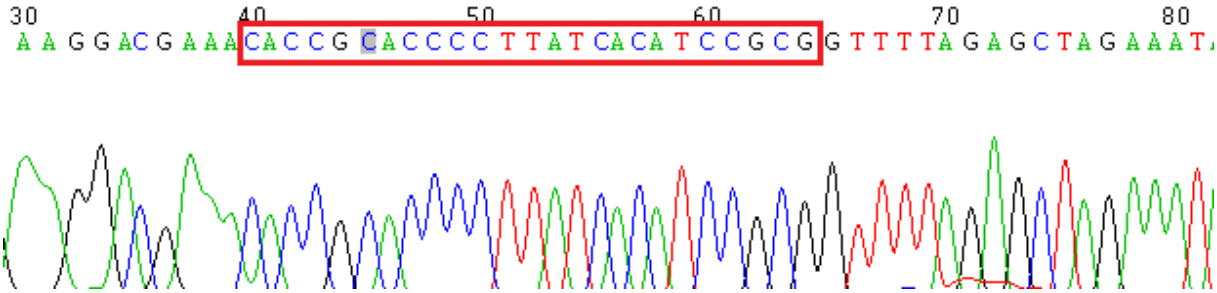

F

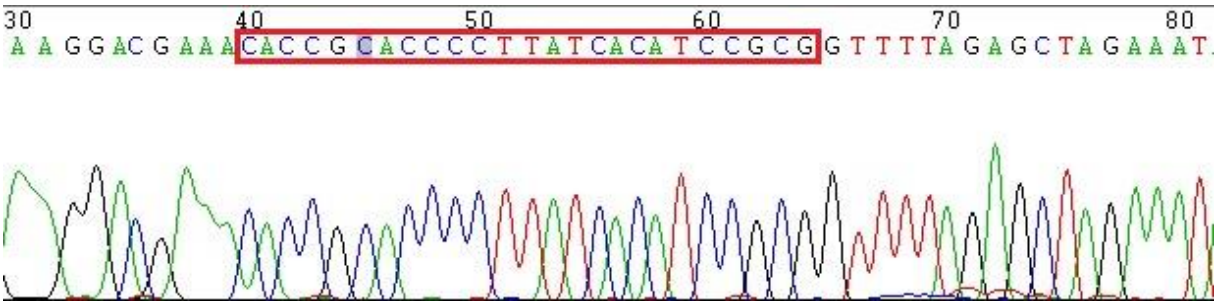

Figure 16: Sequence of the guide sequence oligos cloned into the plasmid. A and B show Guide A forward oligo (highlighted in red box) was successfully cloned into the plasmid; D, E and F show that the sequence of Guide B forward oligo (highlighted in red box) were seamlessly cloned into the plasmid; C did not show the right insertion.

4.3.3 Transfection

The Neon electroporation transfection system was used for transfecting the CRISPR plasmid into NZM17 cells which had the highest Axl expression (**Figure 9**). Electroporation was mainly dependent on the combination of three electric parameters such as the electric field, pulse width, and pulse number. Because there were no available optimized electroporation parameters for our cell type, we first did a 24-well optimization. 24-hours later images were acquired from each well of the plate using a Nikon TE2000 fluorescence microscope. The images were taken separately under brightfield and FITC filters. GFP expression from the CRISPR plasmid was used to show successfully transfected cells. From the images we determined that the best electric parameters for NZM17 were: Pulse voltage--850; Pulse width--30; Pulse no.—2.

Based on the optimized parameters of NZM17, we repeated the transfection, and the fluorescence microscopy images were acquired after 48 hours (**Figure 17**). GFP-expressing cells were apparent in the transfected cultures.

A B C

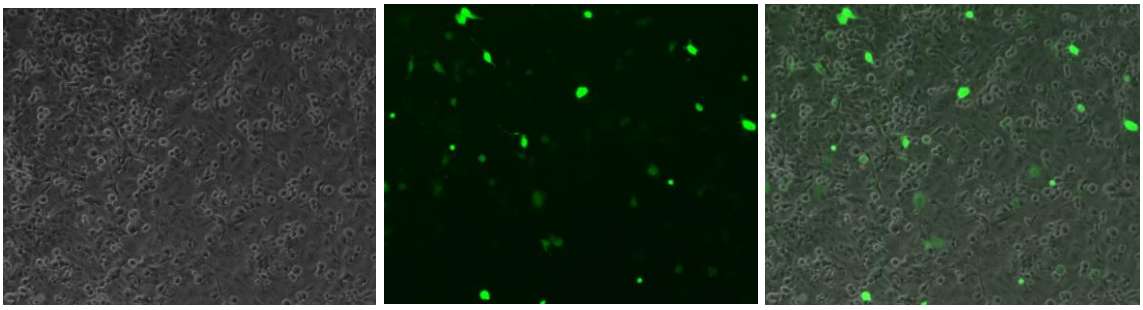

Figure 17: Images of post-transfection NZM17 cells taken by Nikon TE2000 system. A: The monoculture bright field image; B: Fluorescence microscopy image in FITC channel; C: A overlay of A and B. In the pictures of B and C, cells with GFP-expressing (green) cells showed successful transfection by electroporation.

4.4 Analysis of Axl CRISP-knocking out by flow cytometry

4.4.1 Axl knocking out analysis by flow cytometry after GFP sorting.

We analysed the CRISPR plasmid transiently transfected NZM17 cells by flow cytometry to measure Axl and GFP levels and enable enrichment by cell sorting. When the cells in the well reached confluence, we transferred these cells into a small flask in order to expand for sorting. However, the cells grew so fast that the next day, no GFP-expressing cells could be found by fluorescence microscopy. The second time 72 hours after transfection cells grew confluent in the 24-well plate and we directly harvested the cells (around 10^6 cells) and sorted for GFP positive cells (around 7000 cells) by flow cytometor FACS Aria (performed by Marianne Enger). Then the GFP positive cells were cultured and Axl levels were measured by flow cytometry, the data was shown in **Figure 18**. From **Figure 18C** we can find that there was 99.6% of cells still expressed Axl, meaning only 0.4% cells might be Axl knocking out cells.

A B C

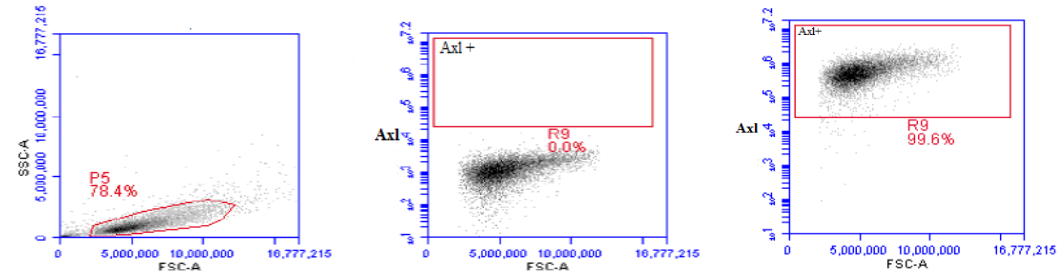

Figure 18: Axl expression by flow cytometry after CRISPR transfection. A: Looking for the right active cells. B: Making a gate of Axl positive/negative expression. C: 99.6% of cells still expressed Axl, indicating only 0.4% cells might be Axl knocking out cells.

4.4.2 Time course analysis of Axl knock out by flow cytometry

To further analyzing the Axl expression of post-CRISPR Axl knock-out plasmid transfection, we harvested the cells from the plate separately at 24 hours, 48 hours and 72 hours after transfection, and analyzed Axl and GPF expression again by flow cytometry. The data is shown in **Figure 19**. From the results we found most cells still expressed Axl (**Figure 19Aa, Ba** and **Ca**); there were some cells transfected with the plasmid and expressed GFP signals (**Figure 19Ab, Bb** and **Cb**). However, the GFP signals decreased over time, consistent with the transient transfection. The desired GFP+ and Axl- cells are not apparent in **Figure 19Ad, Bd** and **Cd,** indicating that the Axl gene was not affected.

A: 24 hours B: 48 hours C: 72 hours

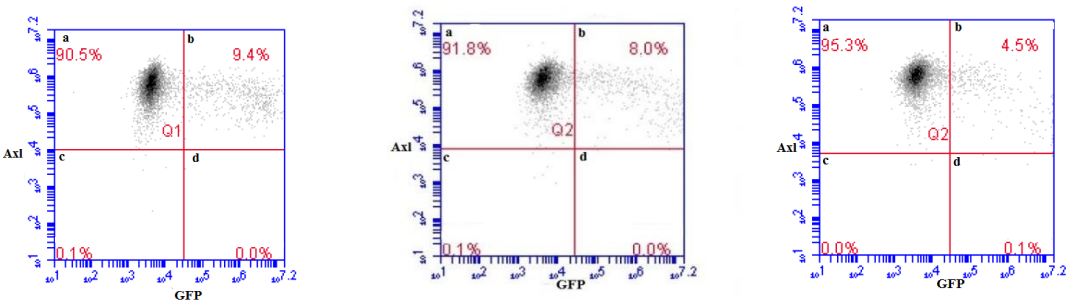

Figure 19: Axl and GFP expression by flow cytometry after CRISPR transfection. In each of A, B and C, there are four areas: a, GFP-/Axl+; b, GFP+/Axl+; c, GFP-/Axl-; d,GFP+/Axl-. Besides, A shows 24hours post transfection; B shows 48 hours post transfection; C shows 72hours post transfection.

Discussion

5.1 Culturing cells at atmospheric oxygen levels impacts cell function.

Common practice for in vitro culture of cells is in incubators where the O_2 tension corresponds to atmospheric levels (21% O_2) [112]. However, the endogenous physiological O_2 tension found in tissues was in the range of 2–5% [113, 114], this discrepancy may lead to misinterpretation of results and it may also be the reason of why effects observed in vitro cannot always be reproduced in vivo and vice versa [112]. According to the previous study results, cell culture O_2 tension was reported significantly impacted on cell proliferation [116], metabolism [117], gene expression [118], inflammation [112], as well as differentiation [119].

According to the data from our cell functions analysis by xCelligence system, we conclude that NZM cells cultured at different oxygen tensions show differences in proliferation and invasiveness; as for migration, the oxygen concentration did not have obvious influence. Yamamoto et al. proved that cells under physiological O_2 tension showed a reduction in the proliferation rate in erythroleukemia cells [120]; Holzwarth et al. also reported that low physiologic oxygen tensions reduce proliferation and differentiation of human multipotent mesenchymal stromal cells [121]. Our data show that cells cultured in atmospheric oxygen level (21% O_2) incubator showed higher proliferation ability than in physiological oxygen level (5% O_2) incubator (**Figure 12**). Furthermore, the invasion ability analysis at both atmospheric and physiological oxygen levels showed important differences. In this study, we showed Akt3 might play inhibitory role in melanoma cell invasion analysis (**Figure 14**), based on the data of NZM40 and NZM86 at physiological oxygen tension (5% O_2). However, at atmospheric oxygen tension the inhibitory role cannot be observed. Besides, similar with proliferation, the invasion ability of the six NZM cell lines was dramatically improved at atmospheric oxygen tension compared with physiological oxygen tension.

To our surprise, in migration assay we failed to show any obvious difference between atmospheric and physiological oxygen levels among the six NZM cell lines. However this needs to be further confirmed. Collectively the data suggested that oxygen concentration should be considered when designing and performing experiments with NZM cells.

5.2 An important role for Axl in melanoma

Emerging evidence suggests that Axl enhances melanoma development by different mechanisms. For instance, Sensi and co-workers detected high Axl expression in 22 of 58 of cell lines (38%) in a melanoma progression panel, and found that Axl promoted tumor cell migration and invasion. Axl knockdown inhibited motility, invasivity, and ability to heal a wound or to migrate across an endothelial barrier [77]. Pharmacological inhibition of Axl using the selective inhibitor BGB324/R428 also showed comparable effects in reducing migration and invasion [77].

However, although Sensi and colleagues showed that Axl depletion did not dramatically affect proliferation, Tworkoski et al. indicated that knockdown of Axl inhibited proliferation

in some lines [78]. Nevertheless, the consensus was that Axl mediated pro-invasive and metastatic behavior in melanoma cells [78]. In addition, Tworkoski et al. also reported increased Axl expression in a subset of melanoma cell lines and tumors relative to melanocytes and showed that targeting Axl reduced melanoma cell proliferation and migration, STAT3 signaling, and in vivo tumor genesis [78]. Furthermore Holland et al. suggested that Axl regulated endothelial tube formation, and implied that Axl may play a role in angiogenesis or vascular mimicry in melanoma [69]. Gjerdrum et al. revealed that EMT program activation led to Axl up-regulation, which was essential for invasiveness and spontaneous metastasis [52]. Recently, Muller et al. proved that inhibition of Axl could lead to melanoma cell death and strongly decrease viability in PLX4720-resistant cells. They also found that a low MITF/Axl ratio predicted resistance to multiple targeted cancer drugs and provide a rationale for clinically exploring Axl inhibitors to combat resistance in MITF-low/Axl high, BRAF and NRAS mutant melanomas [122]. Together these studies support the important role of Axl in melanoma. In our study, we proved that cells with higher Axl expression showed higher proliferation, migration, and relatively high invasion abilities (**Figure 12-14**). Our data agreed with the results of Sensi et al. [77] and Tworkoski et al. [78]. All the results indicated the important role of Axl in melanoma progression and metastasis dissemination.

We will further evaluate the important role of Axl in melanoma cells by cell functional analysis with Axl knock out cells. As our CRISPR results showed that Axl was not successfully knock out (**Figure 18, 19**), the reason leading to the failure was not clear. Although compared with other designer nuclease technologies such as ZFNs and TALENs, Cas9 represents a system that is markedly easier to design, highly specific, efficient and well-suited for high-throughput and multiplexed gene editing for a variety of cell types and organisms [111]. However, in this study, we failed to knock out Axl in NZM17 cells (**Figure 18, 19**). Reasons may include: Cas9 was not expressed, or there was a mutation in the sequence that inhibits the enzyme function; incomplete 2A sequence processing; the gRNA was not expressed properly; the designed gRNA was not optimal; the expression levels of gRNA and Cas9 were insufficient. In this study we used Cas9 nickase mutant (Cas9n) (**Figure 5**) to nick rather than cleave DNA with high specificity, in further study, we will try another CRISPR plasmid including Cas9 nucleases which can carry out strand-specific cleavage with relatively lower specificity but maybe higher efficiency.

5.3 Axl contribution to drug resistance in melanoma.

Melanomas were characterized by activating mutations in BRAF or NRAS, BRAF mutations occur in ~45% of melanoma patients, while NRAS mutations occur in 15–20% of melanoma patients [113]. These mutations activate the downstream kinases MEK and ERK within the MAPK pathway, leading to enhanced cellular proliferation and survival [124]. The discovery of the small-molecule inhibitor vemurafenib, specifically targeting the mutant BRAFV600E kinase, was the first standard of care for patients diagnosed with mutant BRAF metastatic melanoma [125–127]. Although this compound initially reduced tumour burden dramatically,

eventually melanomas became resistant while treatment [128]. Even patients were treated with a combinatorial therapy of BRAF and MEK inhibitors (dabrafenib + trametinib), eventually most patients also became resistant to the treatment [129, 130]. More and more studies found that these resistances in melanoma therapy were associated with Axl. For instance, Muller et al. found that cells which had lost MITF expression after prolonged exposure to BRAF inhibitor PLX4720, showed a strong upregulation of Axl. Besides they also found that increased expression and activity of Axl was seen not only in innate but also acquired resistance of melanoma cells [122]. In addition, Konieczkowski, D. J., et al. indicated that overexpression of Axl was sufficient to confer acquired resistance to RAFi and MEKi [124].

It was reported that Axl expression was detected with a significantly higher frequency in mutant NRAS melanomas [79]. From Kim's results (**Figure 20**), in our six NZM cell lines (highlighted by red diagram), NZM17 and NZM40 showed mutation in NRAS. Both cell lines showed high proliferation, migration and invasion abilities (**Figure 12-14**). Because Axl was also showed be relevant to mutant BRAF cells, it worth further study on the role of Axl in the drug resistance to melanomas with BRAF or NRAS mutations. To further explore the resistant role of Axl in melanoma metastasis therapy, we received new NZM cell lines with BRAF mutation. In future we will perform more study on this direction.

NZM	*BRAF*	*NRAS*	*TP53*	*CDKN2A*	*PIK3CA*
3	V600E			Deletion	
4	V600E		241S/P		
7	V600E		241S/P/WT		
9			179C/T	Deletion	
11	V600E			Deletion	
12	V600E				
13				Deletion	
15		Q61K			
17		Q61K	241S/T		
20	V600E			Deletion	
22			241S/T/W		
23					
26	V600E		136A/G		
28			241S/T/WT + 159a/v		
39			213A/G	Deletion	
40		Q61H	Del 249-253		H1047R
48		Q61K			
49	V600E			Deletion	
50			R280T		
59			Silent T/G	Deletion	
71					
82					
85					
86					
100					

Figure 20: Genetic status of the NZM cell lines. This figure showed different NZM cell lines were detected with different mutations including BRAF and NRAS. The six NZM cell lines used in our study were highlighted by red diagram. NZM17 and NZM40 showed mutation in NARS. Adapted from Reference [115]

5.4 Different roles for Akt3 played in melanoma.

In melanoma tumorigenesis, Akt signaling was proved frequently upregulated [131]. However, Stahl et al. proved that only Akt3, and not Akt1 or Akt2, against by small interfering RNA (siRNA) reduced the amount of phosphorylated (active) Akt in melanoma cells [96], and they also indicated that the predominant isoform Akt3 among Akt family in melanomas, was involved in PI3K/Akt3 pathway and played an important role in melanoma formation, invasion, metastasis and therapeutic resistance [96, 131]. In addition, Madhunapantula et al. also pointed out that activation of Akt3 was a key event regulating the development of melanomas, and enzymes involved in this signaling pathway regulated cell survival, proliferation, metastasis and are implicated in development of resistance to a variety of chemotherapeutic agents [132]. Furthermore, the Akt3 signaling pathway was detected constitutively active in ~70% of advanced-stage melanomas [133]. There was also report proved that overexpression of activated Akt3 enhanced growth of melanoma cells and knockdown of Akt3 remarkably promoted cell apoptosis [98]. It was also well-established that targeting Akt3 inhibited melanoma tumor development, sensitized cells to chemotherapeutic agents and decreased drug resistance [134]. Similarly, studies targeting Akt3 in melanomas using either small interfering RNA or small molecule inhibitors showed that decreased Akt3 activity reduced tumor volume by increasing apoptosis [135, 136].

Our data agree with that higher Akt3 expression enhanced melanoma cells grow and migrate (**Figure 12-13**), however in invasion analysis our data showed ambiguous results. On one hand NZM17 cell lines which had relatively higher expression of Akt3, also showed higher invasion ability in both atmospheric 21% O_2 and physiological 5% O_2; on the other hand the lowest Akt3 expression in gene level (NZM40, **Figure 10**) showed the highest invasion level, and the highest Akt3 expression in protein level (NZM86, **Figure 11**) showed the lowest invasion ability under physiological 5% O_2 condition (**Figure 14**). The results of NZM 40 and NZM86 indicated that Akt3 might inhibit melanoma invasion.

In previous studies, there were also some evidences suggesting that Akt3 exerted inhibitory effects in cancer [83]. For instance, it was reported that Akt3 had been shown to inhibit lung tumor growth in mice and inhibiting Akt3 can lead N-Cadherin to promote breast cancer metastasis [90–92]. However, in melanoma research, this is the first time Akt3 has been found to possibly play an inhibitory role in a melanoma cell invasion analysis.

Similar with Axl, Akt3 was also known can mediate drug resistance. For instance, Akt3 was shown to cooperate with BRAF V600E in the transformation of murine melanocytes in vitro, and directly regulated the activity of mutant BRAF V600E [98]; it was also reported Akt3 mediated resistance to BRAF inhibitor PLX-4720 [134]. In addition, Shao et al. proved Akt3 promoted resistance to apoptosis when BRAF was targeted in melanomas [137]. According to

Kim' data (**Figure 20**) and our data (**Figure 10-14**), later we will also further investigate the resistant role of Akt3 in new NZM cell lines with BRAF mutation, and further detect cell function variation by knocking Akt3 out with CRISPR or inhibiting Akt3 with compounds.

5.5 The Axl-Akt3 signaling pathway may be important in melanoma metastasis.

Tiron et al. in our research group had previously proposed a hypothesis model of Axl-dependent EMT gene program maintenance via activation of nuclear Akt3 based on breast cancer study (**Figure 3**) [102]. As they found that Akt3 was upregulated by EMT and required for Axl-dependent regulation of mammary stem cell traits, besides they also concluded that EMT and stem cell functions required Axl-dependent activation of nuclear targeted Akt3 [102]. They indicated that the Axl-Akt3 signaling pathway might be as a novel therapeutic target to treat advanced breast cancer.

Our study investigated the mechanism for how Axl-Akt3 signaling affected metastasis in melanoma. According to our results, we showed that Axl and Akt3 expression varied in among the six New Zealand Melanoma cell lines (**Figure 7-11**) both in gene and protein level. The most important is that the Axl-Akt3 co-expressing NZM17 cells showed consistent proliferation, migration and invasion abilities both physiological oxygen tension (**Figure 12-14**). As we have discussed above, Akt3 expression in invasion analysis showed two opposite impact: the Axl-Akt3 co-expression cell line NZM17 showed higher invasion ability in both atmospheric 21% O_2 and physiological 5% O_2; but the results of NZM40 and NZM86 (without Axl-Akt3 co-expression) indicated that Akt3 might inhibit melanoma invasion under physiological 5% O_2 condition (**Figure 14**). The reason might be Axl-Akt3 signaling pathway played the key role. Collectively our data suggests that Axl-Akt3 signaling pathway may be important in melanoma metastasis, and targets Axl-Akt3 axis may provide a novel therapy in melanoma metastasis.

Conclusion

In this study, we demonstrated that Axl and Akt3 expression varied in among the New Zealand Melanoma cell lines, furthermore cells with higher expression of Axl showed higher levels of proliferation, migration and invasion; cells with higher expression of Akt3 also showed higher abilities of proliferation and migration, but had the lowest invasion ability without co-expression of Axl. Akt3 might play inhibitory role in melanoma cell invasion analysis at physiological oxygen tension in the absence of Axl. We found that cells kept at different oxygen tensions showed differences in proliferation and invasiveness but similar migration level, and suggested that precise oxygen concentration control should be considered when designing and performing experiments with NZM cells. We elucidated that the Axl-Akt3 signaling pathway may be important in melanoma metastasis, and target the Axl-Akt3 pathway may provide a novel therapy in melanoma metastasis. In conclusion, these results support new therapeutic approaches based on Axl signaling inhibition to treat metastatic melanoma.

In further study, we will retry CRISPR-Cas9 system again with different plasmids again to permanently knock out the Axl gene in the melanoma cell lines to elucidate how Axl signaling contributes melanoma metastasis via Akt3. Furthermore, we will also use available some compounds to inhibit Axl to investigate the drug resistance among NZM cells with BRAF and NARS mutations.

References

1. Eigentler, T. K. and C. Garbe (2006). "Malignant melanoma: classification and staging of malignant melanoma." Front Radiat Ther Oncol 39: 149-158.

2. Lewis, T. B., et al. (2005). "Molecular classification of melanoma using real-time quantitative reverse transcriptase-polymerase chain reaction." Cancer 104(8): 1678-1686.

3. Siegel, R., et al. (2012). "Cancer statistics, 2012." CA Cancer J Clin 62(1): 10-29.

4. World Health Organization (2013) "How common is skin cancer. World Health Organization". Available: http://www.who.int/uv/faq/skincancer/en/index1.html. Accessed 2013 Aug 28

5. Lens, M. B. and M. Dawes (2004). "Global perspectives of contemporary epidemiological trends of cutaneous malignant melanoma." Br J Dermatol 150(2): 179-185.

6. Jemal, A., et al. (2006). "Cancer statistics, 2006." CA Cancer J Clin 56(2): 106-130.

7. Ferlay, J., et al. (2013). "Cancer incidence and mortality patterns in Europe: estimates for 40 countries in 2012." Eur J Cancer 49(6): 1374-1403.

8. Globocan 2008: estimated cancer Incidence, Mortality, Prevalence and Disability-adjusted life years (DALYs) Worldwide in 2008 [Nettside]. Lyon: IARC [oppdatert 2010; lest 1 Nov 2013]. Tilgjengelig fra: http://globocan.iarc.fr/

9. Thompson, J. F., et al. (2005). "Cutaneous melanoma." Lancet 365(9460): 687-701.

10. Gilchrest, B. A., et al. (1999). "The pathogenesis of melanoma induced by ultraviolet radiation." N Engl J Med 340(17): 1341-1348.

11. Fountain, J. W., et al. (1990). "Genetics of melanoma." Cancer Surv 9(4): 645-671.

12. Tucker, M. A., et al. (1997). "Clinically recognized dysplastic nevi. A central risk factor for cutaneous melanoma." JAMA 277(18): 1439-1444.

13. Gandini, S., et al. (2005). "Meta-analysis of risk factors for cutaneous melanoma: III. Family history, actinic damage and phenotypic factors." Eur J Cancer 41(14): 2040-2059.

14. Rhodes, A. R., et al. (1987). "Risk factors for cutaneous melanoma. A practical method of recognizing predisposed individuals." JAMA 258(21): 3146-3154.

15. Gupta, G. P. and J. Massague (2006). "Cancer metastasis: building a framework." Cell 127(4): 679-695.

16. Psaila, B. and D. Lyden (2009). "The metastatic niche: adapting the foreign soil." Nat Rev Cancer 9(4): 285-293.

17. Hanniford, D., et al. (2015). "Identification of metastasis-suppressive microRNAs in primary melanoma." J Natl Cancer Inst 107(3).

18. Chiang, A. C. and J. Massague (2008). "Molecular basis of metastasis." N Engl J Med 359(26): 2814-2823.

19. Chin, L., et al. (2006). "Malignant melanoma: genetics and therapeutics in the genomic era." Genes Dev 20(16): 2149-2182.

20. Tsao, H., et al. (2004). "Management of cutaneous melanoma." N Engl J Med 351(10): 998-1012.

21. Piris, A., et al. (2011). "AJCC melanoma staging update: impact on dermatopathology practice and patient management." J Cutan Pathol 38(5): 394-400.

22. Balch, C. M., et al. (2009). "Final version of 2009 AJCC melanoma staging and classification." J Clin Oncol 27(36): 6199-6206.

23. Azzola, M. F., et al. (2003). "Tumor mitotic rate is a more powerful prognostic indicator than ulceration in patients with primary cutaneous melanoma: an analysis of 3661 patients

24. Schmid-Wendtner, M. H., et al. (2001). "Prognostic index for cutaneous melanoma: an analysis after follow-up of 2715 patients." Melanoma Res 11(6): 619-626.

25. Leiter, U., et al. (2012). "Hazard rates for recurrent and secondary cutaneous melanoma: an analysis of 33,384 patients in the German Central Malignant Melanoma Registry." J Am Acad Dermatol 66(1): 37-45.

26. Balch, C. M., et al. (2001). "Final version of the American Joint Committee on Cancer staging system for cutaneous melanoma." J Clin Oncol 19(16): 3635-3648.

27. American Cancer Society (2012) Cancer Facts & Figures 2012. American Cancer Society Inc.Available:http://www.cancer.org/acs/groups/content/@epidemiologysurveilance/documents/document/acspc-031941.pdf. Accessed 2013 Aug 28

28. Hodi, F. S., et al. (2010). "Improved survival with ipilimumab in patients with metastatic melanoma." N Engl J Med 363(8): 711-723.

29. Robert, C., et al. (2014). "Anti-programmed-death-receptor-1 treatment with pembrolizumab in ipilimumab-refractory advanced melanoma: a randomised dose-comparison cohort of a phase 1 trial." Lancet 384(9948): 1109-1117.

30. Chapman, P. B., et al. (2011). "Improved survival with vemurafenib in melanoma with BRAF V600E mutation." N Engl J Med 364(26): 2507-2516.

31. Hauschild, A., et al. (2012). "Dabrafenib in BRAF-mutated metastatic melanoma: a multicentre, open-label, phase 3 randomised controlled trial." Lancet 380(9839): 358-365.

32. Flaherty, K. T., et al. (2012). "Improved survival with MEK inhibition in BRAF-mutated melanoma." N Engl J Med 367(2): 107-114.

33. Flaherty, K. T., et al. (2012). "Combined BRAF and MEK inhibition in melanoma with BRAF V600 mutations." N Engl J Med 367(18): 1694-1703.

34. Wan, P. T., et al. (2004). "Mechanism of activation of the RAF-ERK signaling pathway by oncogenic mutations of B-RAF." Cell 116(6): 855-867.

35. Long, G. V., et al. (2014). "Combined BRAF and MEK inhibition versus BRAF inhibition alone in melanoma." N Engl J Med 371(20): 1877-1888.

36. Robert, C., et al. (2015). "Improved overall survival in melanoma with combined dabrafenib and trametinib." N Engl J Med 372(1): 30-39.

37. Verma, A., et al. (2011). "Targeting Axl and Mer kinases in cancer." Mol Cancer Ther 10(10): 1763-1773.

38. Korshunov, V. A. (2012). "Axl-dependent signalling: a clinical update." Clin Sci (Lond) 122(8): 361-368.

39. Sasaki, T., et al. (2006). "Structural basis for Gas6-Axl signalling." EMBO J 25(1): 80-87.

40. Stitt, T. N., et al. (1995). "The anticoagulation factor protein S and its relative, Gas6, are ligands for the Tyro 3/Axl family of receptor tyrosine kinases." Cell 80(4): 661-670.

41. Mark, M. R., et al. (1996). "Characterization of Gas6, a member of the superfamily of G domain-containing proteins, as a ligand for Rse and Axl." J Biol Chem 271(16): 9785-9789.

42. McCloskey, P., et al. (1997). "GAS6 mediates adhesion of cells expressing the receptor tyrosine kinase Axl." J Biol Chem 272(37): 23285-23291.

43. Shiozawa, Y., et al. (2010). "GAS6/AXL axis regulates prostate cancer invasion, proliferation, and survival in the bone marrow niche." Neoplasia 12(2): 116-127.

44. Paccez, J. D., et al. (2013). "The receptor tyrosine kinase Axl is an essential regulator of prostate cancer proliferation and tumor growth and represents a new therapeutic target." Oncogene 32(6): 689-698.

45. Zhang, Y. X., et al. (2008). "AXL is a potential target for therapeutic intervention in breast cancer progression." Cancer Res 68(6): 1905-1915.

46. Wimmel, A., et al. (2001). "Axl receptor tyrosine kinase expression in human lung cancer cell lines correlates with cellular adhesion." Eur J Cancer 37(17): 2264-2274.

47. Shieh, Y. S., et al. (2005). "Expression of axl in lung adenocarcinoma and correlation with tumor progression." Neoplasia 7(12): 1058-1064.

48. Linger, R. M., et al. (2013). "Mer or Axl receptor tyrosine kinase inhibition promotes apoptosis, blocks growth and enhances chemosensitivity of human non-small cell lung cancer." Oncogene 32(29): 3420-3431.

49. Neubauer, A., et al. (1993). "Axl, a novel receptor tyrosine kinase isolated from chronic myelogenous leukemia." Semin Hematol 30(3 Suppl 3): 34.

50. Dirks, W., et al. (1999). "Expression of the growth arrest-specific gene 6 (GAS6) in leukemia and lymphoma cell lines." Leuk Res 23(7): 643-651.

51. Hector, A., et al. (2010). "The Axl receptor tyrosine kinase is an adverse prognostic factor and a therapeutic target in esophageal adenocarcinoma." Cancer Biol Ther 10(10): 1009-1018.

52. Gjerdrum, C., et al. (2010). "Axl is an essential epithelial-to-mesenchymal transition-induced regulator of breast cancer metastasis and patient survival." Proc Natl Acad Sci U S A 107(3): 1124-1129.

53. Vuoriluoto, K., et al. (2011). "Vimentin regulates EMT induction by Slug and oncogenic H-Ras and migration by governing Axl expression in breast cancer." Oncogene 30(12): 1436-1448.

54. Byers, L. A., et al. (2013). "An epithelial-mesenchymal transition gene signature predicts resistance to EGFR and PI3K inhibitors and identifies Axl as a therapeutic target for overcoming EGFR inhibitor resistance." Clin Cancer Res 19(1): 279-290.

55. Asiedu, M. K., et al. (2014). "AXL induces epithelial-to-mesenchymal transition and regulates the function of breast cancer stem cells." Oncogene 33(10): 1316-1324.

56. Tsou, A. P., et al. (1998). "Parallel hybridization analysis of multiple protein kinase genes: identification of gene expression patterns characteristic of human hepatocellular carcinoma." Genomics 50(3): 331-340.

57. Xu, M. Z., et al. (2011). "AXL receptor kinase is a mediator of YAP-dependent oncogenic functions in hepatocellular carcinoma." Oncogene 30(10): 1229-1240.

58. Lemke, G. (2013). "Biology of the TAM receptors." Cold Spring Harb Perspect Biol 5(11): a009076.

59. Liu L, et al. (2009). "Novel mechanism of lapatinib resistance in HER2-positive breast tumor cells: activation of AXL". Cancer Res 69, 6871–6878.

60. Zhang Z, et al. (2012). "Activation of the AXL kinase causes resistance to EGFR-targeted therapy in lung cancer." Nat Genet 44, 852–860.

61. Hong J, et al. (2013). "AXL mediates TRAIL resistance in esophageal adenocarcinoma." Neoplasia 15, 296–304.

62. Hong J, et al. (2013). "ABL regulation by AXL promotes cisplatin resistance in esophageal cancer." Cancer Res 73, 331–340.

63. Huang F, et al. (2010). "Differential mechanisms of acquired resistance to insulin-like growth factor-i receptor antibody therapy or to a small-molecule inhibitor, BMS-754807, in a human rhabdomyosarcoma model." Cancer Res 70, 7221–7231.

64. Dufies M, et al. (2011). "Mechanisms of AXL overexpression and function in imatinib-resistant chronic myeloid leukemia cells." Oncotarget 2, 874–885.

65. Gioia R, et al. (2011). "Quantitative phosphoproteomics revealed interplay between Syk and Lyn in the resistance to nilotinib in chronic myeloid leukemia cells." Blood 118, 2211–2221.

66. Lee, H. J., et al. (2014). "Gas6/Axl pathway promotes tumor invasion through the transcriptional activation of Slug in hepatocellular carcinoma." Carcinogenesis 35(4): 769-775.

67. Korshunov, V. A. (2012). "Axl-dependent signalling: a clinical update." Clin Sci (Lond) 122(8): 361-368.

68. Linger, R. M., et al. (2010). "Taking aim at Mer and Axl receptor tyrosine kinases as novel therapeutic targets in solid tumors. Expert Opin. Ther. Targets 14, 1073–1090.

69. Holland, S. J., et al. (2005). "Multiple roles for the receptor tyrosine kinase axl in tumor formation." Cancer Res 65(20): 9294-9303.

70. Linger, R. M., et al. (2008). "TAM receptor tyrosine kinases: biologic functions, signaling, and potential therapeutic targeting in human cancer." Adv Cancer Res 100: 35-83.

71. Son, B. K., et al. (2007). "Gas6/Axl-PI3K/Akt pathway plays a central role in the effect of statins on inorganic phosphate-induced calcification of vascular smooth muscle cells." Eur J Pharmacol 556(1-3): 1-8.

72. Melaragno, M. G., et al. (2004). "Gas6 inhibits apoptosis in vascular smooth muscle: role of Axl kinase and Akt." J Mol Cell Cardiol 37(4): 881-887.

73. Osaki, M., et al. (2004). "PI3K-Akt pathway: its functions and alterations in human cancer." Apoptosis 9(6): 667-676.

74. Engelman, J. A., et al. (2006). "The evolution of phosphatidylinositol 3-kinases as regulators of growth and metabolism." Nat Rev Genet 7(8): 606-619.

75. Bellacosa, A., et al. (2005). "Activation of AKT kinases in cancer: implications for therapeutic targeting." Adv Cancer Res 94: 29-86.

76. Xu, J., et al. (2014). "Axl gene knockdown inhibits the metastasis properties of hepatocellular carcinoma via PI3K/Akt-PAK1 signal pathway." Tumour Biol 35(4): 3809-3817.

77. Sensi M, et al. (2011). "Human cutaneous melanomas lacking MITF and melanocyte differentiation antigens express a functional Axl receptor kinase." J Invest Dermatol 131:2448–57.

78. Tworkoski, K., et al. (2011). "Phosphoproteomic screen identifies potential therapeutic targets in melanoma." Mol Cancer Res 9(6): 801-812.

79. Aplin, A. E. (2011). "Axl of evil?" J Invest Dermatol 131(12): 2343-2345.

80. Masure, S., et al. (1999). "Molecular cloning, expression and characterization of the human serine/threonine kinase Akt-3." Eur J Biochem 265(1): 353-360.

81. Altomare, D. A. and J. R. Testa (2005). "Perturbations of the AKT signaling pathway in human cancer." Oncogene 24(50): 7455-7464.

82. Dillon, R. L. and W. J. Muller (2010). "Distinct biological roles for the akt family in mammary tumor progression." Cancer Res 70(11): 4260-4264.

83. Hers, I., et al. (2011). "Akt signalling in health and disease." Cell Signal 23(10): 1515-1527.

84. Chen, W. S., et al. (2001). "Growth retardation and increased apoptosis in mice with homozygous disruption of the Akt1 gene." Genes Dev 15(17): 2203-2208.

85. Cho, H., et al. (2001). "Insulin resistance and a diabetes mellitus-like syndrome in mice lacking the protein kinase Akt2 (PKB beta)." Science 292(5522): 1728-1731.

86. Easton, R. M., et al. (2005). "Role for Akt3/protein kinase Bgamma in attainment of normal brain size." Mol Cell Biol 25(5): 1869-1878.

87. Tschopp, O., et al. (2005). "Essential role of protein kinase B gamma (PKB gamma/Akt3) in postnatal brain development but not in glucose homeostasis." Development 132(13): 2943-2954.

88. Nakatani, K., et al. (1999). "Identification of a human Akt3 (protein kinase B gamma) which contains the regulatory serine phosphorylation site." Biochem Biophys Res Commun 257(3): 906-910.

89. Turner, K. M., et al. (2015). "Genomically amplified Akt3 activates DNA repair pathway and promotes glioma progression." Proc Natl Acad Sci U S A 112(11): 3421-3426.

90. Chung, S., et al. (2013). "N-cadherin regulates mammary tumor cell migration through Akt3 suppression." Oncogene 32(4): 422-430.

91. Hollander, M. C., et al. (2011). "Akt1 deletion prevents lung tumorigenesis by mutant K-ras." Oncogene 30(15): 1812-1821.

92. Linnerth-Petrik, N. M., et al. (2014). "Opposing functions of Akt isoforms in lung tumor initiation and progression." PLoS One 9(4): e94595.

93. Kulawiec, M., et al. (2009). "Cancer cell mitochondria confer apoptosis resistance and promote metastasis." Cancer Biol Ther 8(14): 1378-1385.

94. Robertson, G. P. (2005). "Functional and therapeutic significance of Akt deregulation in malignant melanoma." Cancer Metastasis Rev 24(2): 273-285.

95. Stahl, J. M., et al. (2003). "Loss of PTEN promotes tumor development in malignant melanoma." Cancer Res 63(11): 2881-2890.

96. Stahl, J. M., et al. (2004). "Deregulated Akt3 activity promotes development of malignant melanoma." Cancer Res 64(19): 7002-7010.97. Madhunapantula, S. V., et al. (2009). "The PTEN-AKT3 signaling cascade as a therapeutic target in melanoma." Pigment Cell Melanoma Res 22(4): 400-419.

98. Cheung, M., et al. (2008). "Akt3 and mutant V600E B-Raf cooperate to promote early melanoma development." Cancer Res 68(9): 3429-3439.

99. Julien, S., et al. (2007). "Activation of NF-kappaB by Akt upregulates Snail expression and induces epithelium mesenchyme transition." Oncogene 26(53): 7445-7456.

100. Dhawan, P., et al. (2002). "Constitutive activation of Akt/protein kinase B in melanoma leads to up-regulation of nuclear factor-kappaB and tumor progression." Cancer Res 62(24): 7335-7342.

101. Madhunapantula, S. V., et al. (2007). "PRAS40 deregulates apoptosis in malignant melanoma." Cancer Res 67(8): 3626-3636.

102. Tiron, C., et al. (2014). "Axl regulates normal and transformed mammary epithelial plasticity via nuclear targeted Akt3." Manuscript submitted.

103. Marshall, E. S., et al. (1994). "Radiosensitivity of new and established human melanoma cell lines: comparison of [3H]thymidine incorporation and soft agar clonogenic assays." Eur J Cancer 30A(9): 1370-1376.

104. Kim, J. E., et al. (2012). "Comparison of growth factor signalling pathway utilisation in cultured normal melanocytes and melanoma cell lines." BMC Cancer 12.

105. Xing, J. Z., et al. (2005). "Dynamic monitoring of cytotoxicity on microelectronic sensors." Chem Res Toxicol 18(2): 154-161.

106. Cho, S.W., et al. (2013). Targeted genome engineering in human cells with the Cas9 RNA-guided endonuclease. Nat. Biotechnol. 31, 230–232.

107. Cong, L., et al. (2013). "Multiplex genome engineering using CRISPR/Cas systems." Science 339(6121): 819-823.

108. Dong, S., et al. (2015). "Heritable CRISPR/Cas9-Mediated Genome Editing in the Yellow Fever Mosquito, Aedes aegypti." PLoS One 10(3): e0122353.

109. Pellagatti, A., et al. (2015). "Application of CRISPR/Cas9 genome editing to the study and treatment of disease." Arch Toxicol.

110. Ran, F. A., et al. (2013). "Genome engineering using the CRISPR-Cas9 system." Nat Protoc 8(11): 2281-2308.

111. Brown, M. and C. Wittwer (2000). "Flow cytometry: principles and clinical applications in hematology." Clin Chem 46(8 Pt 2): 1221-1229.

112. Haas, B., et al. (2015). "Permanent culture of macrophages at physiological oxygen attenuates the antioxidant and immunomodulatory properties of dimethyl fumarate." J Cell Physiol 230(5): 1128-1138.

113. Tsai, A. G., et al. (2003). "Oxygen gradients in the microcirculation." Physiol Rev 83(3): 933-963.

114. Carreau, A., et al. (2011). "Why is the partial oxygen pressure of human tissues a crucial parameter? Small molecules and hypoxia." J Cell Mol Med 15(6): 1239-1253.

115. Kim, J. E., et al. (2013). "Heterogeneity of expression of epithelial-mesenchymal transition markers in melanocytes and melanoma cell lines." Front Genet 4: 97.

116. Atkuri, K. R., et al. (2005). "Culturing at atmospheric oxygen levels impacts lymphocyte function." Proc Natl Acad Sci U S A 102(10): 3756-3759.

117. Parrinello, S., et al. (2003). "Oxygen sensitivity severely limits the replicative lifespan of murine fibroblasts." Nat Cell Biol 5(8): 741-747.

118. Wood, I. S., et al. (2011). "Modulation of adipokine production, glucose uptake and lactate release in human adipocytes by small changes in oxygen tension." Pflugers Arch 462(3): 469-477.

119. Grodzki, A. C., et al. (2013). "Oxygen tension modulates differentiation and primary macrophage functions in the human monocytic THP-1 cell line." PLoS One 8(1): e54926.

120. Yamamoto, Y., et al. (2014). "Triiodothyronine suppresses activin-induced differentiation of erythroleukemia K562 cells under hypoxic conditions." Mol Cell Biochem 391(1-2): 217-224.

121. Holzwarth, C., et al. (2010). "Low physiologic oxygen tensions reduce proliferation and differentiation of human multipotent mesenchymal stromal cells." BMC Cell Biol 11: 11.

122. Muller, J., et al. (2014). "Low MITF/AXL ratio predicts early resistance to multiple targeted drugs in melanoma." Nat Commun 5: 5712.

123. Scolyer, R.A., et al. (2011). "Evolving concepts in melanoma classification and their relevance to multi-disciplinary melanoma patient care." Mol. Oncol. 5, 124–136.

124. Konieczkowski, D. J., et al. (2014). "A melanoma cell state distinction influences sensitivity to MAPK pathway inhibitors." Cancer Discov 4(7): 816-827.

125. Chapman, P. B., et al. (2011). "Improved survival with vemurafenib in melanoma with BRAF V600E mutation." N Engl J Med 364(26): 2507-2516.

126. Tsai, J., et al. (2008). "Discovery of a selective inhibitor of oncogenic B-Raf kinase with potent antimelanoma activity." Proc Natl Acad Sci U S A 105(8): 3041-3046.

127. Bollag, G., et al. (2010). "Clinical efficacy of a RAF inhibitor needs broad target blockade in BRAF-mutant melanoma." Nature 467(7315): 596-599.

128. Wagle, N., et al. (2011). "Dissecting therapeutic resistance to RAF inhibition in melanoma by tumor genomic profiling." J Clin Oncol 29(22): 3085-3096.

129. Shi, H., et al. (2014). "A novel AKT1 mutant amplifies an adaptive melanoma response to BRAF inhibition." Cancer Discov 4(1): 69-79.

130. Wagle, N., et al. (2014). "MAP kinase pathway alterations in BRAF-mutant melanoma patients with acquired resistance to combined RAF/MEK inhibition." Cancer Discov 4(1): 61-68.

131. Robertson, G. P. (2005). "Functional and therapeutic significance of Akt deregulation in malignant melanoma." Cancer Metastasis Rev 24(2): 273-285.

132. Madhunapantula, S. V. and G. P. Robertson (2011). "Therapeutic Implications of Targeting AKT Signaling in Melanoma." Enzyme Res 2011: 327923.

133. Soengas, M. S. and S. W. Lowe (2003). "Apoptosis and melanoma chemoresistance." Oncogene 22(20): 3138-3151.

134. Madhunapantula, S. V., et al. (2011). "The Akt signaling pathway: an emerging therapeutic target in malignant melanoma." Cancer Biol Ther 12(12): 1032-1049.

135. Krasilnikov, M., et al. (1999). "Contribution of phosphatidylinositol 3-kinase to radiation resistance in human melanoma cells." Mol Carcinog 24(1): 64-69.

136. Sun, M., et al. (2001). "AKT1/PKBalpha kinase is frequently elevated in human cancers and its constitutive activation is required for oncogenic transformation in NIH3T3 cells." Am J Pathol 159(2): 431-437.

137. Shao, Y. and A. E. Aplin (2010). "Akt3-mediated resistance to apoptosis in B-RAF-targeted melanoma cells." Cancer Res 70(16): 6670-6681.